Author's response by Wenjie Wang et al.

Corresponding to mshao@pku.edu.cn.

We greatly appreciate the time and efforts that the Referees spent in reviewing our manuscript. The comments are really thoughtful and helpful to improve the quality of our paper. We have addressed each comment below, with the Referee comment in black text, our response in blue text, and relevant manuscript changes noted in red text.

I think the main difference is that aeronet ssa represent the column and in situ ssa what happens near the ground plus the drying that you mention. I think this have to be clarified.

Response: Many thanks, and I have clarified it. As we used the measured hygroscopic factor (Liu et al., 2009) and measured RH to correct the SSA, the drying didn't contribute to the difference.

The 11%-16% due to SSA in situ / aeronet differences you are mentioning is very important. It means that due to the in situ SSA use, you are constantly underestimating the PFs by this amount. I think this have to be reported.

Response: Many thanks. I have added this part in the manuscript.

However, if you have a look at the following paper of Krotkov et al.
https://www.researchgate.net/publication/237741790_Aerosol_ultraviolet_absorption_experiment_2002_to_2004_part_2_Absorption_optical_thickness_refractive_index_and_single_scattering_albedo/figures, and Corr et al.,
https://www.atmos-chem-phys.net/9/5813/2009/
they point out that SSA in the UV can be lower than the visible. So in general this 11-16% could be less.

Response: Many thanks. I have added this part in the manuscript.

Line 408-426:

It worth noting that the mean near-ground SSA (525nm) in August 2012 (0.88±0.08) is significantly lower than the mean AERONET based SSA (440nm) in the same period (0.94±0.02) and in summer (0.94±0.02). The different wavelength plays a minor role in the different SSA according to the wavelength dependence of

AERONET based SSA in the range of 440-1020 nm (Figure S3). This difference is mainly because that the AERONET based SSA represents the column and in situ SSA happens near the ground. The effect of the difference in SSA (0.88 vs 0.94) results in photolysis frequencies changing by 11%-16% according to TUV model. It means that due to the in situ SSA use, the photolysis frequencies tend to be underestimated. Krotkov et al. (2005) and Corr et al. (2009) pointed out that SSA in the UV can be lower than the visible. So in general this 11-16% could be less. The AERONET based SSA generally reproduces well the slope of $j(O^1D)$ versus AOD in spite that it significantly underestimates the absolute value of the slope at low AOD range (AOD<0.7), which is probably due to the uncertainty of AERONET based SSA in low AOD range. In addition to the uncertainty of SSA, both of SSA at 440nm and at 525nm differ from the 305-315nm wavelength range of $j(O^1D)$, which is likely to lead to some uncertainties for the analysis of the relationship between $j(O^1D)$ and AOD.

Line 718-722:

Corr, C. A., Krotkov, N., Madronich, S., Slusser, J. R., Holben, B., Gao, W., Flynn, J., Lefer, B., Kreidenweis, S. M.: Retrieval of aerosol single scattering albedo at ultraviolet wavelengths at the T1 site during MILAGRO. ATMOSPHERIC CHEMISTRY AND PHYSICS, 9, 5813-5827, DOI: 10.5194/acp-9-5813-2009, 2009.

The impact of aerosols on photolysis frequencies and ozone production in urban Beijing during the four-year period 2012–2015

Wenjie Wang[1], Xin Li[1*], Min Shao[1,2*], Min Hu[1], Limin Zeng[1], Yusheng Wu[1], Tianyi Tan[1]

1 State Joint Key Laboratory of Environmental Simulation and Pollution Control, College of Environmental Sciences and Engineering, Peking University, Beijing 100871, China

2 Institute for Environmental and Climate Research, Jinan University, Guangzhou 511443, China

*** Correspondence to:**

Xin Li (li_xin@pku.edu.cn)

Min Shao (mshao@pku.edu.cn)

Abstract

During the period 2012-2015, the photolysis frequencies were measured at the Peking University site (PKUERS), a representative site of urban Beijing. We present a study of the effects of aerosols on two key photolysis frequencies, $j(O^1D)$ and $j(NO_2)$. Both $j(O^1D)$ and $j(NO_2)$ display significant dependence on AOD (380nm) with a nonlinear negative correlation. With the increase in AOD, the slopes of photolysis frequencies vs AOD decrease, which indicates that the capacity of aerosols to reduce the actinic flux decreases with AOD. The absolute values of slopes are equal to 4.2-6.9▪10^{-6} s^{-1} and 3.4▪10^{-3} s^{-1} per AOD unit for $j(O^1D)$ and $j(NO_2)$ respectively at SZA of 60° and AOD smaller than 0.7, both of which are larger than those observed in a similar, previous study in the Mediterranean. This indicates that the aerosols in urban Beijing have a stronger extinction effect on actinic flux than absorptive dust aerosols in the Mediterranean. Since the photolysis frequencies strongly depended on the AOD and the solar zenith angle (SZA), we established a parametric equation to quantitatively evaluate the effect of aerosols on photolysis frequencies in Beijing. According to the parametric equation, aerosols lead to a decrease in seasonal mean $j(NO_2)$ by 24% and 30% for summer and winter, respectively, and the corresponding decrease in seasonal mean $j(O^1D)$ by 27% and 33% respectively, compared to an aerosol-free atmosphere (AOD = 0). Based on an observation campaign in August 2012, we used the photochemical box model to simulate the ozone production rate ($P(O_3)$). The simulation results shows that the monthly mean daytime net ozone production rate is reduced by up to 25% due to the

light extinction of aerosols. Through further in-depth analysis, it was found that particulate matter concentrations maintain high level under the condition of high concentrations of ozone precursors (VOCs and NOx), which inhibits the production of ozone to a large extent. This phenomenon implies a negative feedback mechanism in the atmospheric environment of urban Beijing.

1. Introduction

Solar radiation plays an important role in atmospheric photochemistry, driving the photolysis of many key species. The photolysis of ozone (O_3), gaseous nitrous acid (HONO), and carbonyl species, which contributes to the primary production of HOx (Volkamer et al., 2010). The photolysis of ozone produces O^1D, which then reacts with H_2O to form OH radicals; these radicals are the main source of OH radicals in the troposphere, as shown by reactions R1 and R2. The strong dependence of OH concentration on $j(O^1D)$ was found in a number of field measurements (Ehhalt et al., 2000; Rohrer et al., 2014; Stone et al., 2012). In addition, the photolysis of NO_2 produces O^3P, and then O^3P reacts with O_2 to produce O_3, as shown by reactions R3 and R4, which is the only significant chemical source of ozone in the troposphere (Finlayson-Pitts et al., 2000). The photolysis frequencies of R1 and R3 are $j(O^1D)$ and $j(NO_2)$, respectively.

$$O_3 + h\nu \ (\lambda < 330\ nm) \rightarrow O^1D + O_2 \quad \text{(R1)}$$

$$O^1D + H_2O \rightarrow 2OH \quad \text{(R2)}$$

$$NO_2 + h\nu\ (\lambda < 430\ nm) \rightarrow NO + O^3P \quad \text{(R3)}$$

$$O^3P + O_2 \rightarrow O_3 \quad \text{(R4)}$$

The photolysis frequencies are calculated by the following formula:

$$j = \int_{\lambda_1}^{\lambda_2} F(\lambda)\sigma(\lambda, T)\varphi(\lambda, T)\,\mathrm{d}\lambda \quad \text{(E1)}$$

F(λ) is the actinic flux dependent on wavelength. Since the photolysis rates are proportional to the actinic flux and not all stations acquire a 2π spectroradiometer or chemical actinometers for J measurements, several methods have been developed to determine actinic flux and photolysis frequencies from ground based measurements of irradiance (Kylling et al 2003, Kazadzis et al. 2000, 2004, Topaloglou et al. 2005, Trebs et al. 2009). σ(λ, T) is the absorption cross section of the species that absorbs in the wavelength range λ_1-λ_2. φ(λ, T) is the quantum yield of the photodissociation reaction product. λ, and T represent wavelength, species and temperature, respectively.

The effect of aerosols on photolysis frequencies depends on the aerosol optical properties, SZA and altitude (Liao et al., 1999). The aerosol optical depth (AOD) characterizes the integral of the extinction coefficient of aerosols in the vertical direction. The light extinction of aerosols includes scattering and absorption, which have different effects on the actinic flux. Previous studies showed that scattering aerosols can enhance the actinic flux throughout the troposphere, while absorptive aerosols reduce the actinic flux throughout the boundary layer (Jacobson, 1998; Dickerson et al., 1997; Castro et al., 2001; Flynn et al., 2010). To distinguish

between these two components, single scattering albedo (SSA) is defined as the ratio of the scattering coefficient to the total extinction coefficient. In areas with severe aerosol pollution, aerosols can significantly affect photolysis frequencies and ozone production. Studies in Los Angeles (Jacobson, 1998), Mexico City (Castro et al., 2001; Raga et al., 2001; Li et al., 2011), São Paulo (de Miranda et al., 2005), Huston (Flynn et al., 2010), Europe (Real et al., 2011) and Russia (Pere et al., 2015) have found that aerosols reduce ozone concentration by 5-30% by attenuating photolysis frequencies. Studies in the eastern United States have shown that scattering aerosols increase ozone concentration by 5-60% by increasing the photolysis frequencies (Dickerson et al., 1997; He and Carmichael, 1999). Therefore, it is necessary to quantitatively evaluate the effect of aerosols on photolysis frequencies for a better understanding of ozone formation under highly polluted conditions.

Currently, the methods for quantitatively evaluating the influence of aerosols on photolysis frequencies mainly include radiative transfer model and parameterization method (Madronich et al., 1993). Radiative transfer model is based on an algorithm for calculating solar radiation and photolysis frequencies (Madronich et al., 1999). The observed data of related influential factors of the photolysis frequencies are taken as the model's input to calculate the photolysis frequencies. This method comprehensively considers the influence of aerosol optical properties on the photolysis frequencies, but it does not necessarily reflect the true quantitative relationship in the atmosphere due to complicated environmental conditions and thus the simulated results don't necessarily reproduce observed values well (Lefer et al.,

2003; Shetter et al., 2003; Hofzumahaus et al., 2004). For example, the simulated slope of $j(O^1D)$ vs AOD by Fast-JX algorithm within the CHIMERE model was significantly smaller than the observed slope, particularly for the high SZA values (Mailler et al., 2016). The parameterization method is based on the observation data taken from a certain region and is used to establish the parameterized relationship between the photolysis frequencies and optical properties of aerosols (such as AOD). The method can reflect the actual atmospheric environment conditions; it also considers less influential factors and thus is easy to apply (Casasanta et al., 2011; Gerasopoulos et al., 2012). The disadvantage of this method is that the established parametric equations apply only to a specific region and cannot be extended to other regions.

With rapid economic development and urbanization in past decades, China's atmospheric pollution has become more and more severe, characterized by high concentrations of particulate matter and ozone. Satellite observations indicates that both the particulate matter and the ozone of eastern China are at higher levels compared with other locations in the globe (Verstraeten et al., 2015; Ma et al., 2014). Levels of pollution in the Beijing–Tianjin–Hebei are even more severe (Chang et al., 2009; Che et al., 2008; Zhang et al., 2014, Zhang et al., 2016). Therefore, it is necessary to study the effects of aerosols on photolysis frequencies and ozone production in the urban areas of China.

Previous model studies have shown that aerosols in China can affect ozone production by changing the photolysis frequencies. Tang et al. (2004) used a sulfur

transmission–emission model (STEM) to discover that ozone concentration in northeastern China was reduced by 0.1–0.8% in the sandstorm due to the change in photolysis frequencies . Tie et al. (2005) used a global aerosol–chemical model to show that aerosols caused $j(O^1D)$ and $j(NO_2)$ to decrease in winter by 20%-30% and 10%-30%, respectively, and in summer by 5%-20% and 1%-10%, respectively, resulting in 2%-5% and 2% reductions in ozone concentration in winter and summer, respectively. Li et al. (2011) used an air quality model to estimate the changes in the photolysis frequencies caused by sulfate, nitrate, ammonium, and mineral dust aerosols in the central and eastern regions of China from June 1 to June 12, 2006. This study showed that the daily average $j(O^1D)$ in the troposphere at the altitude of 1 km, 3 km, and 10 km from the ground was reduced by 53%, 37-%, and 21%, respectively, resulting in a decrease in the ozone concentration by 5.4%, 3.8%, and 0.10% in the three layers. Lou et al (2014) found that with aerosols, annual mean photolysis frequencies , $j(O^1D)$) and $j(NO_2)$, were simulated to be reduced by 6-18% in polluted eastern China, leading to reductions in O_3 of up to 0.5 ppbv in those regions in spring and summer by using the global chemical transport model (GEOS-Chem). However, all of these studies base their results on model simulations. Research using long-term observational data to evaluate the effects of aerosols on photolysis frequencies and ozone production in China has not yet been published.

Our overall goal is to quantitatively evaluate the effect of aerosols in urban Beijing on photolysis frequencies and thus on ozone production. First, the relationship between $PM_{2.5}$ and AOD was investigated. Second, based on long-term

observations (2012-2015) of photolysis frequencies, we discussed the impact of AOD on photolysis frequencies ($j(O^1D)$ and $j(NO_2)$) in urban Beijing in detail. The relationship between photolysis frequencies and AOD is adequately compared with previous study in the Mediterranean (Casasanta et al., 2011; Gerasopoulos et al., 2012). Then, the quantitative relationship between photolysis frequencies, AOD, and SZA was acquired by the parameterization method, which could be used to quantitatively evaluate the effect of AOD on photolysis frequencies in Beijing. Finally, a photochemistry box model was used to evaluate the effect of aerosols on ozone production.

2. Methodology

2.1. Measurement

From August 2012 to December 2015, $j(O^1D)$ and $j(NO_2)$ were measured continuously at PKUERS site. The data of the period during October 2012 to March 2013 and August 2015 are missed due to instrument maintenance and other measurement campaigns. The site (39.99°N, 116.31°E) is located on the sixth floor of a campus building at the Peking University, 20 km northwest of Tiananmen Square. The height from the ground is about 30 m. The sampling point is surrounded by classroom buildings. Concentration level and composition of air pollutants were thought to be similar to the downtown so as to be representative for the whole of Beijing (Wang et al., 2010; Xu et al., 2011; Zhang et al., 2012; Zhang et al., 2014).

The actinic flux was measured using a spectroradiometer and the photolysis frequencies were calculated from the absorption cross section and quantum yield of each species (Shetter and Müller, 1999). The spectroradiometer consisted of a single monochromator with a fixed grating (CARL ZEISS), an entrance optic with a 2π steradian (sr) solid angle quartz diffusor and a 2048×64-pixel photodiode array detector. The spectral measurements were performed with a wavelength resolution of 2 nm, covering a wavelength range of 290-650 nm (Hofzumahaus et al., 1999). A 1000 W National Institute of Standard and Technology (NIST) traceable lamp was used for calibration under laboratory conditions (Bohn et al., 2008). The measured spectra were corrected for dark signal and stray light. For $j(O^1D)$, the quantum yields used were taken from Matsumi et al.(2002), while the ozone cross section was derived from Daumont et al. (1992) and Malicet et al. (1995). Measured temperatures were used to retrieve ozone absorption cross section and quantum yield. For $j(NO_2)$, the quantum yields used were taken from Bass et al. (1976) and Davenport et al. (1978), while the cross section was derived from Jones and Bayes (1973), Harker et al. (1977) and Davenport (1978). The calculated photolysis frequencies had a time resolution of 10 s and an accuracy of ±10% including uncertainties associated with the quartz receiver and stray-light effects (Edwards and Monks, 2003).

The optical properties of aerosols were measured by a CIMEL solar photometer (AERONET level 2 data collection, http://aeronet.gsfc.nasa.gov/) and the site selected is the Beijing-CAMS site (39.93°N, 116.32°E), which is 6.4km from the

PKUERS site. The CIMEL solar photometer is an automatic solar-sky scanning radiometer that uses selected spectral channels. The instrumentation, data acquisition, retrieval algorithms, and calibration procedure conform to the standards of the AERONET global network and have been described in detail by Fotiadi et al. (2006). The solar extinction measurement was performed every 3 minutes in the spectral range 340–1020 nm for the calculation of AOD at wavelengths 340, 380, 440, 500, 675, 870, 970, and 1020 nm. Under cloudless conditions, the overall uncertainty of AOD data is ± 0.01 at $\lambda > 440$ nm and ± 0.02 at shorter wavelengths. In this study, AOD at the wavelength of 380 nm was chosen for analysis. This wavelength was selected as it is more representative of $j(NO_2)$. Additionally, at this wavelength we can better compare with the results of Gerasopoulos et al. (2012). The daytime clear-sky conditions were identified according to the presence of AOD data of AERONET since AOD data are unavailable under cloudy conditions. AE and SSA (440nm) were also acquired from ARONET. In addition, the SSA (525nm) data were derived from a field campaign undertaken in August 2012. The absorption and scattering coefficients were measured with an Aethalometer (AE-31, Magee) and a Single Wavelength Integrating Nephelometer (Aurora-1000), respectively, with a time resolution of 1 minute. As aerosol particles were dried by decreasing relative humidity (RH) to <40% when SSA was measured, we used the measured hygroscopic factor (Liu et al., 2009) and measured RH to correct the SSA. Five-minute averages of AOD, SSA, and photolysis frequencies were analyzed in this study. The total ozone column was obtained by OMI (Ozone Monitoring

Instrument) for the year 2012-2015, using overpass data (http://www.temis.nl/protocols/O3global.html) (Henk et al., 2003). In addition, meteorological parameters such as temperature, relative humidity, and pressure were simultaneously observed at this site. Table 1 presents total O_3 column, temperature, relative humidity, daytime clear-sky fraction and respective standard deviation for different seasons.

The analysis of the effects of aerosols on ozone production (Section 3.4) was based on the field campaign undertaken in August 2012. The relevant contents and methods of observation are shown in Table 2. Since the time resolution of VOCs is 1 hour, all data analyzed in Section 3.4 was processed as 1-hour average values. In this study, we focused on the effects of aerosols on photolysis frequencies and ozone production under cloudless conditions.

2.2 Radiative Transfer Model Description

We use the Tropospheric Ultraviolet and Visible (TUV) radiation model (version 5.3) provided by Sasha Madronich (Madronich, 1993). In order to solve the radiative transfer equation, TUV uses the discrete-ordinates algorithm (DISORT) with 4 streams and calculates the actinic flux spectra with wavelength range of 280-420 nm in 1 nm steps and resolution. Measured temperatures were used to calculate the absorption cross sections and quantum yields. The key aerosol optical properties including AOD, SSA and AE were input into the model to test the effect of aerosols on photolysis frequencies. AE(380/550nm) is taken from AERONET and the mean value of 1.2 during June 2012 - December 2015 is used in TUV model.

2.3 Photochemical box model

The photochemical box model used in this study is based on a regional atmospheric chemical mechanism (RACM2) described by Goliff et al. (2013). The mechanism includes 17 stable inorganic compounds, 4 intermediate inorganic compounds, 55 stable organic compounds, and 43 intermediate organic compounds. Compounds not specifically treated in RACM are incorporated into species with similar functional groups. The isoprene-related mechanism used in this model is LIM mechanism proposed by Peeters et al. (2009). In this study, the observed NO_2, CO, SO_2, C2–C12 NMHCs, HCHO, photolysis frequencies, temperature, pressure, and relative humidity were used as constraints to simulate the concentrations of reactive radicals (RO_2, HO_2, and OH), intermediate species, and associated reaction rate constants. HONO wasn't measured during the period and was calculated according to the concentration of NO_2 and the observed ratio of HONO to NO_2 at an urban site in Beijing, which had a marked diurnal cycle, a maximum in the early morning (ratio values up to ~0.05–0.08 in summer) and a decrease during daytime to values around 0.01–0.02 (Hendrick et al., 2014). The model was spun up for two days once it started running in order to ensure that the simulation was stable. It was assumed that the lifetime of simulated species removed by dry deposit was 24 hours. The lifetime corresponds to the assumed deposit rate of 1.2 cm s^{-1} and a well-mixed boundary layer height of about 1 km (Lu et al., 2012). Net ozone production is equal

to the reaction rate between peroxy radicals (RO_2 and HO_2) and NO minus the loss rate of NO_2 and O_3 as shown in E2, E3, and E4 as derived by Mihelcic et al. (2003). The ozone production rate ($P(O_3)$), the ozone loss rate ($D(O_3)$), and the net $P(O_3)$ were calculated from the simulation results.

$$P(O_3) = k_{HO2+NO}[HO_2][NO] + \sum\left(k^i{}_{RO2+NO}\left[RO^i{}_2\right][NO]\right) \quad \text{(E2)}$$

$$D(O_3) = (\theta j(O^1D) + k_{OH+O3}[OH] + k_{HO2+O3}[HO_2] + \sum(k^j{}_{alkene+O3}[alkene^j]))[O_3] + k_{OH+NO2}[OH][NO_2] \quad \text{(E3)}$$

$$net\ P(O_3) = P(O_3) - D(O_3) \quad \text{(E4)}$$

where θ is the fraction of O^1D from ozone photolysis that reacts with water vapor. i and j represent the number of species of RO_2 and alkenes, respectively.

3. Results and discussion

3.1 The correlation between $PM_{2.5}$ and AOD

Compared with AOD, $PM_{2.5}$ is a more common proxy to evaluate the level of particulate matter pollution in spite that AOD is a more closely related parameter of photolysis frequencies. As a result, we attempted to analyze the quantitative relationship between $PM_{2.5}$ and AOD to evaluate the influence of $PM_{2.5}$ on AOD and

thus on photolysis frequencies. The factors that affect this relationship include aerosol type, aerosol size distribution, aerosol distribution in the vertical direction, relative humidity (RH) and planetary boundary layer height (PBLH) (van Donkelaar et al., 2010). Figure 1 shows the correlation between AOD and $PM_{2.5}$ in four different seasons. The determination coefficient (r^2) is 0.53, 0.58, 0.62 and 0.59 for spring (March, April and May), summer (June, July and August), autumn (September, October and November) and winter (December, January and February), respectively. Meanwhile, the correlation exhibits significant seasonal differences, having relatively smaller slope (23.56) in summer and relatively larger slope (73.76) in winter. This implies that $PM_{2.5}$ in summer has stronger light extinction capacity than in winter. One reason for the seasonal differences is the variation in RH among different seasons (Table 1). There is higher RH in summer (57.2% on average) than in winter (30.4% on average), leading to stronger hygroscopic growth of aerosol particles, and thus resulting in higher scattering ability of aerosol particles. According to another study in urban Beijing, the higher the RH, the smaller the slope, and the higher the PBLH, the smaller the slope (Zheng, C. W et al., 2017). In addition, the slope was smaller for scattering-dominant aerosols than for absorbing-dominant aerosols, and smaller for coarse mode aerosols than for fine mode aerosols (Zheng, C. W et al., 2017). The slopes of the correlation between AOD (at 550nm) and $PM_{2.5}$ in this study in summer and winter are equal to 42.2μg m^{-3} and 119.2μg m^{-3}, respectively, close to that from Ma et al. (2016) (54.9μg m^{-3} and 110.5μg m^{-3}) and Xin et al. (2016) (55.2 μg m^{-3} and 93.4μg m^{-3}), but smaller

significantly than that from Zheng et al. (2017) (65~74μg m^{-3} and 143~158μg m^{-3}). The differences mainly depend on the aerosol composition and size distribution at different observational sites in Beijing. Compared with other cities in North China (Tianjin, Shijiazhuang and Baoding) (Ma et al., 2016), the slope in Beijing for winter is significantly higher. Consequently, using $PM_{2.5}$ to estimate AOD has a large uncertainty due to multiple interference factors.

3.2 Seasonal and diurnal variability of AOD and photolysis frequencies

The diurnal cycles of AOD are shown in Figure 2. AOD displays obvious diurnal variation, with relatively high level at noon and low level at dawn and evening. The diurnal variation of $PM_{2.5}$ is significantly different from AOD. In addition, AOD has obvious seasonal differences, with the highest AOD in summer and the lowest AOD in winter. Conversely, $PM_{2.5}$ in winter (42μg m^{-3}) is significantly higher than in summer (35μg m^{-3}). In spite of lower $PM_{2.5}$ in summer, AOD in summer is higher due to stronger extinction capacity of $PM_{2.5}$ as discussed in 3.1. Figure 3 shows the diurnal variation of the photolysis frequencies under cloudless conditions for each season. $j(O^1D)$ and $j(NO_2)$ are both highest in summer, followed by spring and autumn, and lowest in winter. This seasonal difference is mainly determined by the difference in SZA for the four seasons.

The observed mean daily maxima of photolysis frequencies at this site are lower than that observed in the eastern Mediterranean (Crete, Greece, 35°20′N, 25°

40′E) (Gerasopoulos et al., 2012) by $7.8\times10^{-6} \pm 5.5\times10^{-6}$ s^{-1} and $5.5\times10^{-6} \pm 1.8\times10^{-6}$ s^{-1} for $j(O^1D)$, and $1.9\times10^{-3} \pm 1.2\times10^{-3}$ s^{-1} and $3.3\times10^{-3} \pm 1.0\times10^{-3}$ s^{-1} for $j(NO_2)$, in summer and winter respectively. The corresponding lower photolysis frequencies of Beijing than the eastern Mediterranean due to SZA difference is 1.7×10^{-6} s^{-1} and 3.0×10^{-6} s^{-1} for $j(O^1D)$, and 8.0×10^{-5} s^{-1} and 6.6×10^{-4} s^{-1} for $j(NO_2)$ according to TUV model under aerosol-free conditions, which are significantly lower than observed decreased magnitudes. Additionally, we know that the temperature is lower in Beijing during the winter compared to conditions in Crete. The measured mean temperature in Beijing during winter is equal to 0.53±4.2 ℃ (Table 1). When we consider the temperature in Crete is 10 ℃ higher than in Beijing, the lower $j(O^1D)$ of Beijing than Crete is 5.5×10^{-7} s^{-1}, which is also not able to compensate the $j(O^1D)$ gap between the two sites during winter. Taking into account the similar levels of ozone column concentration in the two sites, the large gap of photolysis frequencies in the two sites is mainly attributed to the higher AOD in Beijing (0.76±0.75) than in the eastern Mediterranean (0.27±0.13).

It can be seen from Figure 3 that the difference between winter and summer for $j(O^1D)$ is significantly larger than that for $j(NO_2)$, where the summer midday averages of $j(O^1D)$ and $j(NO_2)$ are 5 times and 2 times those of winter, respectively. There are two reasons for this phenomenon. One, compared with $j(NO_2)$, $j(O^1D)$ is more sensitive to the change in SZA and the same change in SZA results in a larger change in $j(O^1D)$ than $j(NO_2)$. Two, the main influential factors of $j(NO_2)$ under cloudless conditions are SZA and AOD, and the influence of ozone column

concentration and temperature on $j(NO_2)$ is negligible. However, $j(O^1D)$ is affected significantly by the ozone column concentration and temperature, in addition to SZA and AOD. The higher ozone column concentration and lower temperature in winter than in summer lead to the difference in $j(O^1D)$ further increasing (Table 1).

3.3 The correlation between photolysis frequencies and AOD

3.3.1 The correlation between $j(O^1D)$ and AOD

In order to rule out the effect of SZA on photolysis frequencies, we chose SZA equal to 30° and 60° (± 1°) for analysis. Figure 4 presents the dependence of $j(O^1D)$ on AOD at different levels of ozone column concentration at SZA of 30° and 60° (± 1°). The ozone column concentration has a classification width of 30 DU. This relatively large classification width is chosen to make sure that there are enough points to fit the relationship between $j(O^1D)$ and AOD. $j(O^1D)$ exhibits a clear dependence on AOD, with a nonlinear negative correlation. The scatter of these points is mainly due to variations in ozone column and temperature. As AOD increased, the slope of $j(O^1D)$-AOD gradually decreases, indicating that the ability of aerosols to reduce $j(O^1D)$ gradually decreases with AOD. This result differs from that found in Mediterranean, where $j(O^1D)$ was linearly negatively correlated with AOD (Casasanta et al., 2011; Gerasopoulos., 2012). A larger variation range of AOD in Beijing (0-3) compared with Mediterranean (0-0.6) is one reason for the difference.

For further analysis, the observed relation between $j(O^1D)$ and AOD was compared with TUV-simulated results. Panels a and b of Figure 5 present the comparison between observed and TUV-simulated $j(O^1D)$ against AOD at a SZA of 30° and 60° respectively and ozone column concentration of 330-360 DU. The observed $j(O^1D)$ was at ozone column of 330-360DU and were scaled to the temperature of 298K. AE(380/550nm) = 1.2, ozone column = 345 and Temperature = 298K were used in TUV model for all simulations. Mean Earth-Sun distance was used in the calculations of TUV model and measured j-values were scaled to the mean Earth-Sun distance. At low AOD level (< 0.8), the observed slope of $j(O^1D)$ vs AOD is significantly larger than the simulated slope at SSA of 0.95, and slightly larger than the simulated slope at SSA of 0.85. With AOD increasing, the observed slope decreases rapidly to the level smaller than the simulated slopes.

The rapid change of the slope with AOD can be related to the variation of SSA at different AOD level. Figure 6 presents the relationship between SSA and AOD. Figure 6 (a) presents the relationship between AERONET based SSA (440nm) and AOD during 2012-2015. The result suggests a significant positive correlation between SSA and AOD. Additionally, Figure 6 (b) also presents a significant positive correlation between near-ground SSA (525nm) from measurement campaign in August 2012 and AOD. With the increase in AOD, SSA is elevated; meanwhile, the slope of SSA vs AOD is gradually reduced. Similar results in other regions have been obtained by Bais et al., 2005, Krotkov et al., 2005 and Kazadzis et al., 2012. SSA characterizes the ratio of the scattering extinction coefficient to the total

391 extinction coefficient (scattering extinction coefficient plus absorptive extinction
392 coefficient) of aerosols. The smaller the SSA, the higher the absorptive component
393 and lower the scattering component of the aerosol, and the stronger the ability of the
394 aerosol to reduce the actinic flux (Dickerson et al., 1997). Figure 6 indicates that
395 aerosols in Beijing under low AOD conditions had a higher proportion of absorptive
396 aerosol components than under high AOD conditions, and, as a result, had a stronger
397 ability to reduce the photolysis frequencies, which contributed to the rapidly reduced
398 slope of $j(O^1D)$ vs AOD with AOD. However, due to absence of more SSA data of
399 the period 2012-2015, we can't give more sufficient evidence for the dependence of
400 SSA on AOD. For another perspective, Owing to the biomass burning and soot
401 emission generated from heating, the fine mode heavily-absorbing aerosol
402 percentage is higher in winter than in summer (Zheng et al., 2017; Liu et al., 2016;
403 Zhang et al., 2013), and thus aerosols in winter have stronger ability to reduce the
404 photolysis frequencies. Table S1 indicates that SSA in summer is higher significantly
405 than in winter. High AOD levels often appeared in summer and low AOD levels
406 occurred mostly in winter (Figure 2 and Table S1), another fact that may also
407 explains the rapidly reduced slope of $j(O^1D)$ vs AOD with AOD.

408 It worth noting that the mean near-ground SSA (525nm) in August 2012
409 (0.88±0.08) is significantly lower than the mean AERONET based SSA (440nm) in
410 the same period (0.94±0.02) and in summer (0.94±0.02). The different wavelength
411 plays a minor role in the different SSA according to the wavelength dependence of
412 AERONET based SSA in the range of 440-1020 nm (Figure S3). This difference is

possiblymainly because that due to the AERONET based SSA represents the column and in situ SSA happens near the groundthe uncertainty of AERONET based SSA and the poor vertical representative of near-ground SSA. The effect of the difference in SSA (0.88 vs 0.94) results in photolysis frequencies changing by 11%-16% according to TUV model. It means that due to the in situ SSA use, the photolysis frequencies tend to be underestimated. Krotkov et al. (2005) and Corr et al. (2009) pointed out that SSA in the UV can be lower than the visible. So in general this 11-16% could be less. The AERONET based SSA generally reproduces well the slope of $j(O^1D)$ versus AOD in spite that it significantly underestimates the absolute value of the slope at low AOD range (AOD<0.7), which is probably due to the uncertainty of AERONET based SSA in low AOD range. In addition to the uncertainty of SSA, both of SSA at 440nm and at 525nm differ from the 305-315nm wavelength range of $j(O^1D)$, which is likely to lead to some uncertainties for the analysis of the relationship between $j(O^1D)$ and AOD.

Comparing panels a and b of Figure 4, we see that at AOD smaller than 1, the slope of $j(O^1D)$ vs AOD exhibits a significant dependence on SZA and the slope at 30° of SZA is about 1.5-2.0 times larger than that at 60° of SZA. This result is similar to that of the observations made in the central Mediterranean (Casasanta et al., 2011). For the purpose of comparison with the study in the Mediterranean, the slope of $j(O^1D)$ vs AOD was calculated at AOD smaller than 0.7.

Table 3 presents slope, intercept and the determination coefficient (r^2) of linear fits of correlation between $j(O^1D)$ and AOD for each ozone column class at AOD

smaller than 0.7. At SZA of 60° and O_3 column concentration of 300-330 DU, the respective slope of the linear regression indicates a reduction of $j(O^1D)$ by $4.2 \cdot 10^{-6}$ s^{-1} per AOD unit. Gerasopoulos et al. (2012) reported that the observed slope in the eastern Mediterranean was equal to $2.4 \cdot 10^{-6}$ s^{-1} at O_3 column of 300-320 DU. Casasanta et al. (2011) reported that the observed slope in the central Mediterranean varied from $2.7 \cdot 10^{-6}$ s^{-1} to $3.9 \cdot 10^{-6}$ at O_3 column of 300-330 DU. All of these results are smaller than the value of the present study, indicating that aerosols in urban Beijing had a stronger extinction capacity on $j(O^1D)$ than those in the Mediterranean that was influenced by both natural absorptive aerosols and anthropogenic aerosols. Previous study indicated that SSA in Beijing ranged from 0.80 to 0.86 (Garland et al., 2009;Han et al., 2015b; Han et al., 2017; Tian et al., 2015). The relatively low SSA in Beijing could be an important reason for the stronger extinction capacity.

3.3.2 The correlation between $j(NO_2)$ and AOD

Unlike $j(O^1D)$, $j(NO_2)$ is negligibly affected by ozone column concentration and depends mainly on AOD and SZA under cloudless conditions. Figure 7 presents the dependence of $j(NO_2)$ on AOD at different SZA levels under cloudless conditions. The cosine of SZA (cos (SZA)) is categorized according to a width of 0.2. In the same category of cos (SZA), $j(NO_2)$ displays a strong dependence on AOD. The scatter of these points is due to the relatively large classification width of SZA to a

large extent. When cos(SZA) is at its maximum level (0.8-1), the correlation between $j(NO_2)$ and AOD is close to linear. When cos (SZA) decreases, the correlation tends to be nonlinear. Similar to $j(O^1D)$, the observed slopes of $j(NO_2)$ vs AOD are also larger than TUV-simulated slope at SSA of 0.95 and 0.85 when AOD is smaller than 0.8, and decreased rapidly with increasing AOD (panels c and d of Figure 5). The reason for this result is the same with that for $j(O^1D)$ as explained above.

Table 4 presents the slope, intercept and the determination coefficient (r^2) of linear fits of correlation between $j(NO_2)$ and AOD for each ozone column class at AOD smaller than 0.7. The slope of $j(NO_2)$ vs AOD also displays a significant dependence on cos(SZA). The slope increases as cos(SZA) increases from 0 to 0.5 and then decreases as cos(SZA) increases from 0.5 to 1. At SZA of 60°±1 (cos(SZA)=0.5±0.015), the respective slope of the linear regression indicates a reduction of $j(NO_2)$ by $3.4 \cdot 10^{-3}$ s^{-1} per AOD unit. This result is larger than the value for non-dust aerosols ($2.2 \cdot 10^{-3}$ s^{-1}) and close to the value for dust aerosols ($3.1 \cdot 10^{-3}$ s^{-1}) in the eastern Mediterranean reported by Gerasopoulos et al. (2012).

3.4 The parameterization relationship between photolysis frequencies, AOD, and SZA

As analyzed above, the photolysis frequencies ($j(O^1D)$ and $j(NO_2)$) strongly depended on AOD and cos(SZA) and could be fit into expression E5 using a quadratic polynomial form. The fitting parametric equations for $j(NO_2)$ is shown in Table 5. For $j(O^1D)$, both of O_3 column and temperature affect $j(O^1D)$ significantly. Figure S1 presents the dependence of $j(O^1D)$ on ozone column at low AOD level (AOD<0.3) and SZA of (a) 30°±1° and (b) 60°±1°, respectively. Ozone column ranging from 270 to 400 DU leads to $j(O^1D)$ reducing about 50%. In order to evaluate the impact of temperature on $j(O^1D)$, we calculated the ratio of $j(O^1D)$ at measured temperature to $j(O^1D)$ at temperature = 298K ($j(O^1D)/ j(O^1D)_{T=298K}$) (Figure S2). $j(O^1D)/j(O^1D)_{T=298K}$ varied from 0.82 to 1.03 indicating that temperature changed $j(O^1D)$ by no more than 21%. Therefore, temperature played a minor role in changing $j(O^1D)$ compared with ozone column. As a result, when we fitted the relationship among $j(O^1D)$, AOD and cos(SZA), the effect of ozone column is considered but the effect of temperature is not considered. By fitting the relationship at different ozone classes (classification width=30DU), we found that ozone column increasing by 30DU results in $j(O^1D)$ at a constant SZA and AOD decreasing by 18%. Therefore, the parametric equation for $j(O^1D)$ is transformed into the form E6, which reflects the influence of ozone column. The parameters a_1-a_6 correspond to ozone column range = 300-330 DU, thus we use 315 DU as the weighted standard of ozone column. The fitting parameters a_1-a_6 for $j(O^1D)$ is shown in Table 6.

$$j(NO_2) = a_1 + a_2 AOD + a_3 cos(SZA) + a_4 (AOD)^2 + a_5 AOD cos(SZA) + a_6 (cos(SZA))^2 \quad \text{E5}$$

498 $$j(O^1D) = [a_1 + a_2 AOD + a_3 cos(SZA) + a_4 (AOD)^2 + a_5 AOD cos(SZA) + a_6 (cos(SZA))^2] \times [1+(315 - O_3 \text{ column}) \times 0.006]$$

499 ..... E6

500 The coefficients of determination of the fitting equations are greater than 0.95
501 for $j(NO_2)$ and $j(O^1D)$ at a certain O_3 column, indicating that both of the photolysis
502 frequencies strongly depended on AOD and cos(SZA), and the effect of other factors
503 such as SSA and AE are integrated into the constant term in the parametric equation.
504 Since the ozone column concentration has greater influence on $j(O^1D)$ than on
505 $j(NO_2)$, the parameters of fitting equations for $j(NO_2)$ are similar, but the parameters
506 of fitting equations for $j(O^1D)$ have a large fluctuation at different O_3 column ranges
507 (especially a_1 and a_2). The parametric equations can be used to quantitatively
508 evaluate the effect of AOD on photolysis frequencies in Beijing. According to the
509 parametric equations, aerosols lead to a decrease in seasonal mean $j(NO_2)$ by 24%
510 and 30% and a decrease in seasonal mean $j(O^1D)$ by 27% and 33% in summer and
511 winter under clear-sky conditions, respectively, compared to an aerosol-free
512 atmosphere. The decreasing ratio of the photolysis frequencies in winter is higher
513 than in summer mainly due to the higher SZA in winter.

514

515 The effect of aerosols on photolysis frequencies in Beijing is compared with
516 other studies. Real and Sartelet (2011) reported a reduction in $j(NO_2)$ and $j(O^1D)$ of
517 13%-14% due to aerosols by using the radiative transfer code Fast-J during summer
518 2001 over European regions. Flynn et al (2010) reported that aerosols reduced $j(NO_2)$
519 by 3% in Huston during 2006 by using TUV model. Gerasopoulos et al (2012)

reported that aerosols reduced j(NO_2) and j(O^1D) by 5%-15% with 5-yr mean AOD at 380nm equal to 0.27. All of these results are lower than the reduction ratio of this study mainly due to higher aerosol level in Beijing (4-yr mean AOD equal to 0.76± 0.75). Hodzic et al. (2007) simulated a 15–30% j(NO_2) photolysis reduction during the 2003 European summer heatwave in the case of absorbing biomass burning aerosols with AOD at 550 nm equal to 0.7-0.8 and SSA at 532 nm equal to 0.83-0.87. The result of Hodzic et al. (2007) is comparable with the reduction ratio of this study possibly due to the equivalent levels of AOD and SSA. In addition, Péré et al (2015) simulated a higher reduction (20–50%) in j(NO_2) and j(O^1D) along the transport of the aerosol plume during the 2010 Russian summer wildfires episode. The higher reduction is due to the higher level of AOD (peak value of AOD at 400nm reached 2-4), even though SSA is very high (0.97).

3.5 The influence of AOD on ozone production

In order to explain the effect of aerosol light extinction on ozone production, we used the data from the field observation campaign undertaken in August 2012. Ozone production depends on its precursors (NOx and VOCs), meteorological factors, and solar radiation. Solar radiation is the driving force for tropospheric photochemical reactions, in which j(O^1D) and j(NO_2) are both important for ozone production. On the one hand, the increase in j(NO_2) promotes the photolysis of NO_2,

thereby accelerating the formation of ozone. On the other hand, the increase in $j(O^1D)$ accelerates the photolysis of ozone. In addition, the increase in the photolysis frequencies will accelerate the photolysis of OVOC (especially formaldehyde and acetaldehyde), HONO, and H_2O_2, resulting in increases in OH and HO_2, which will promote the reaction between OH and VOCs and thus produce more RO_2. As a result, more ozone is produced by increasing the reaction rate between RO_2 (or HO_2) and NO. However, the increase in OH and HO_2 also consumes ozone and NO_2, which contributes to the increase in $D(O_3)$. In brief, the overall effect of changes in photolysis frequencies on sources and sinks of ozone determines the change in the net ozone production rate.

Ozone production (HO_2 + NO, RO_2 + NO), ozone loss ($O^1D + H_2O$, $HO_2 + O_3$, O_3 + OH, NO_2 + OH, and O_3 + alkenes), and net ozone production rate during August 2012 were calculated by using the box model. We used the observed photolysis frequencies (i.e. j_obs) and the calculated photolysis frequencies by parametric equation under the condition of AOD equal to 0 (i.e. j_AOD=0), were used to constrain the box model. The difference of simulated results in the two scenarios can be attributed to the effect of aerosol light extinction. As a result, the presence of aerosols causes a decrease in both ozone production rate and loss rate, as is shown in Figure 8. Since the decreasing amplitude of the daytime ozone production rate is far larger than that of the daytime ozone loss rate, the mean daytime net production rate of ozone is reduced by 25%. This reduction is comparable with the results of the study in Mexico City, where aerosols caused a 20%

563 reduction in the ozone concentrations (Castro et al., 2001). Studies in Houston and
564 Crete have shown that aerosols cause ozone production rates to decrease by about 4%
565 and 12%, respectively, which are lower than that found in this study (Flynn et al.,
566 2010; Gerasopoulos et al., 2012).

567 The ratio of the observed photolysis frequencies to the photolysis frequencies at
568 AOD equal to 0 is defined as JIF (Flynn et al., 2010). A JIF of less than 1 indicates
569 that the aerosols cause a decrease in the photolysis frequencies. Figure 9 shows the
570 relation between $P(O_3)_{j\_obs}/P(O_3)_{j\_AOD=0}$ (or $D(O_3)_{j\_obs}/D(O_3)_{j\_AOD=0}$) and JIF. The
571 majority of JIF values were less than 1, with an average of 0.72, indicating that
572 aerosols greatly attenuated photolysis frequencies due to high levels of AOD
573 (average of 1.07) ~~and low levels of SSA (average of 0.88)~~ during the observation
574 period. $P(O_3)_{j\_obs}/P(O_3)_{j\_AOD=0}$ and $D(O_3)_{j\_obs}/D(O_3)_{j\_AOD=0}$ are both linearly
575 positively correlated with JIF and the scatters are mostly above the 1:1 line. As can
576 be seen from the figure 9, a 30% reduction in photolysis frequencies (JIF = 0.7) due
577 to the presence of aerosols results in a decrease in ozone production rate and loss rate
578 by about 26% and 15%, respectively. The decreasing amplitude in the ozone
579 production rate is greater than the decrease in the ozone loss rate because the
580 corresponding processes of ozone production are all light-driven, but the
581 corresponding processes of ozone loss are not all light-driven because the reaction of
582 O_3 with alkenes does not depend on solar radiation. According to the simulated
583 results, the reaction of ozone with alkenes during this campaign accounts for 17% of
584 total ozone loss.

585 The diurnal profile of the mean ozone production and loss rate is shown in
586 Figure 10. $P(O_3)$ peak midday in the 12:00-14:00 local hours at 31 ppb/h without
587 aerosol impact and 23 ppb/h with aerosol impact. The maximum $D(O_3)$ also occurrs
588 between 12:00 and 14:00 at 4.2 ppb/h without aerosol impact and 3.5 ppb/h with
589 aerosol impact. There is little difference between aerosol-impact and aerosol-free
590 $P(O_3)$ (or $D(O_3)$) in the hours of 6:00-11:00, but the difference in the afternoon
591 (12:00-18:00) is large, indicating that the reduction effect of aerosol on ozone
592 production mainly occurs during the afternoon.
593 The above analysis focuses on the effect of aerosol on the ozone production due
594 to aerosol light extinction. However, it does not consider the close relationship
595 between aerosol and ozone's gaseous precursors in the actual atmosphere. To explain
596 this problem, we chose two adjacent days (small SZA effect) with obviously
597 different AOD levels: a clean day (A day: August 21, 2012; AOD = 0.21, $PM_{2.5}$=21.6
598 $\mu g\ m^{-3}$) and a day with high aerosol pollution (B day; August 26, 2012; AOD = 3.2,
599 $PM_{2.5}$=125.0 $\mu g\ m^{-3}$) (Table 7). The difference in AOD between the two days can be
600 taken to represent the maximum daytime gap of AOD for this month. The ozone
601 column concentrations for these two days were 302 DU and 301 DU, respectively, of
602 which the effect on $j(O^1D)$ is negligible. Under these conditions, the $j(O^1D)$ value at
603 noon time decreases from $3.23 \times 10^5\ s^{-1}$ on A day to $1.29 \times 10^5\ s^{-1}$ on B day (i.e., a 60%
604 reduction) and the $j(NO_2)$ value at noon time decreases from $8.26 \times 10^{-3}\ s^{-1}$ on A day
605 to $4.19 \times 10^{-3} s^{-1}$ on B day (i.e., a 49.2% reduction). As shown in Table 7, B day has
606 higher AOD and higher concentrations of gaseous pollutants. The concentrations of

607 CO, NO_2, HCHO and the OH reactivity of VOCs in B day are much higher than in A
608 day, with the ratio of 3.6, 2.3, and 2.0, respectively. The simultaneous increases of
609 gaseous pollutants and AOD are due to the fact that gaseous pollutants (NOx, SO_2,
610 and VOCs) emitted by major pollution sources in Beijing, including traffic and
611 industry, have undergone the processes of gas-phase oxidation and nucleation to
612 generate secondary particulate matter that contributes to aerosol light extinction.
613 Previous studies have reported that secondary particulate matter has accounted for
614 more than 60% of total particulate matter during severe smog pollution in Beijing
615 summers (Han et al., 2015a; Guo et al., 2014). In addition, several studies have
616 shown that secondary components in particulate matter (especially secondary
617 organics and ammonium sulfate) have dominated the aerosol light extinction (Han et
618 al., 2014; Han et al., 2017; Wang et al., 2015). Observations made in Beijing during
619 the summer of 2006 showed that ammonium sulfate and ammonium nitrate
620 contributed 44.6% and 22.3%, respectively, to the total extinction coefficient during
621 a severe period of smog (Han et al., 2014); in the summer of 2014 in Beijing,
622 ammonium sulfate, secondary organic aerosols, and ammonium nitrate contributed
623 30%, 22%, and 18%, respectively, to the total extinction coefficient (Han et al.,
624 2017).

625 As shown in Figure 11, the simulation results indicate that the net $P(O_3)$ of B
626 day is 36.2% higher than that of A day due to higher concentrations of ozone
627 precursors on B day. This result is consistent with the observed ozone concentrations,
628 of which the observed ozone concentration in B day is 2.2 times higher than that of

A day. If we adjust the photolysis frequencies level of B day to the level of A day, the net $P(O_3)$ increases by 70.0%, which indicates that the high level of particulate matter in B day greatly inhibits ozone production. This result means that the system is under negative feedback, thus keeping O_3 at a relatively stable level. Table 8 summarizes the average levels of gaseous pollutants and photolysis frequencies for AOD less than 1 and greater than 1, as measured during August 2012. It shows that, the concentrations of ozone's precursors are higher and the photolysis frequencies are lower at high AOD levels (AOD > 1) than those at low AOD level (AOD < 1). This result means that the negative feedback mechanism is prevalent throughout the whole campaign period. Therefore, the prevention and control measures of air pollution in Beijing need to incorporate this coupling mechanism between particulate matter and ozone to achieve effective control of these two main pollutants.

4. Conclusion

Photolysis reactions are important driving forces for tropospheric photochemical oxidation processes and ozone production. In this study, we explored in detail the effects of aerosols on photolysis frequencies and ozone production in Beijing, based on a long observation period of 4 years. We have found that:

(1) There is a strong correlation between $PM_{2.5}$ and AOD, and the slope in summer is smaller significantly than in winter, which indicates that aerosols in summer have a more efficient extinction capacity than in winter.

649 (2) As AOD increased, the extinction effect of aerosol on photolysis
650 frequencies was decreased; this result was probably related to a higher
651 proportion of scattering aerosols under high AOD conditions than under low
652 AOD conditions. The slope of the correlation between photolysis
653 frequencies and AOD indicates that the aerosols in urban Beijing have a
654 stronger extinction on actinic flux than absorptive dust aerosols in the
655 Mediterranean.
656 (3) The influence of AOD on photolysis frequencies was evaluated
657 quantitatively by establishing parametric equations. According to the
658 parametric equation, aerosols lead to a decrease in seasonal mean $j(NO_2)$ by
659 24% and 30% for summer and winter, respectively, and the corresponding
660 decrease in seasonal mean $j(O^1D)$ by 27% and 33% respectively, compared
661 to an aerosol-free atmosphere.
662 (4) In order to evaluate the effects of aerosols on ozone production rate, we
663 carried out an observation campaign in August 2012. The results show that
664 aerosols reduced the net ozone production rate by 25% by reducing the
665 photolysis frequencies. High concentrations of ozone gaseous precursors
666 were often accompanied by high concentrations of particulate matter, which,
667 to a large extent, inhibited excessive levels of ozone generation and
668 reflected the negative feedback effect of the atmospheric system. Therefore,
669 the influence of aerosol on photolysis frequencies and thus on the rate of
670 oxidation of VOCs and NOx to ozone and secondary aerosol is important

for determining the atmospheric effects of controlling the precursor emissions of these two important air pollutants (aerosols and ozone).

Author contribution

Author	Contribution
Wenjie Wang	acquisition of data; analysis and interpretation of data; drafting the article and revising it critically
Min Shao	substantial contributions to conception and design; revising the article critically
Xin Li	substantial contributions to conception and design; revising the article critically
Min Hu	collection of data
Limin Zeng	collection of data
Yusheng Wu	collection of data
Tianyi Tan	collection of data

ACKNOWLEDGEMENTS

This work was supported by the Major Program of the National Natural Science Foundation of China [Grant number 91644222]. We thank Hongbin Chen and Philippe Goloub for data management of AOD and other aerosol optical properties on AERONET.

Reference

Barnarda, J. C., Chapmana E G., Fasta, J. D., Schmelzera, J. R., Slusserb, J. R., Shetterc, R. E.: An evaluation of the FAST-Jphotolysis algorithm for predicting nitrogen dioxide photolysis rates under clear and cloudy sky conditions, ATMOSPHERIC ENVIRONMENT, 38, 3393-3403, 10.1016/j.atmosenv.2004.03.034, 2004.

Bais, A. F., Kazantzidis, A., Kazadzis, S., Balis, D. S., Zerefos, C. S., Meleti, C.: Deriving an effective aerosol single scattering albedo from spectral surface UV irradiance measurements, ATMOSPHERIC ENVIRONMENT, 39, 1093-1102, DOI: 10.1016/j.atmosenv.2004.09.080, 2005.

Bass, A. M., Ledford, A, E., and Laufer, A. H.: Extinction coefficients of NO_2 and N_2O_4, J. Res. Nat. Bureau Standards, 80A, 143-162, 1976.

Bohn, B., Corlett, G. K., Gillmann, M., Sanghavi, S., Stange, G., Tensing, E., Vrekoussis, M., Bloss, W. J., Clapp, L. J., Kortner, M., Dorn, H. P., Monks, P. S., Platt, U., Plass-Dulmer, C., Mihalopoulos, N., Heard, D. E., Clemitshaw, K. C ., Meixner, F. X., Prevot, A. S. H., Schmitt, R.: Photolysis frequency measurement techniques: Results of a comparison within the ACCENT project, ATMOSPHERIC CHEMISTRY AND PHYSICS, 8, 5373–5391, doi:10.5194/acp-8-5373-2008, 2008.

Casasanta, G., di Sarra, A., Meloni, D., Monteleone, F., Pace, G., Piacentino, S., Sferlazzo, D.: Large aerosol effects on ozone photolysis in the Mediterranean, ATMOSPHERIC ENVIRONMENT, 45, 3937-3943, 10.1016/j.atmosenv.2011.04.065, 2011.

Castro, T., Madronich, S., Rivale, S., Muhlia, A., Mar, B.: The influence of aerosols on photochemical smog in Mexico City, ATMOSPHERIC ENVIRONMENT, 35, 1765-1772, 10.1016/S1352-2310(00)00449-0, 2001.

Chang, D., Song, Y., Liu, B.: Visibility trends in six megacities in China 1973–2007, ATMOSPHERIC RESEARCH, 94, 161-167, 10.1016/j.atmosres.2009.05.006,

2009.

Che, H., Zhang, X., Li, Y., Zhou, Z., Qu, J. J., Hao, X.: Haze trends over the capital cities of 31 provinces in China, 1981–2005, THEORETICAL AND APPLIED CLIMATOLOGY, 97, 235-242, 10.1007/s00704-008-0059-8, 2009.

Corr, C. A., Krotkov, N., Madronich, S., Slusser, J. R., Holben, B., Gao, W., Flynn, J., Lefer, B., Kreidenweis, S. M.: Retrieval of aerosol single scattering albedo at ultraviolet wavelengths at the T1 site during MILAGRO. ATMOSPHERIC CHEMISTRY AND PHYSICS, 9, 5813-5827, DOI: 10.5194/acp-9-5813-2009, 2009.

de Miranda, R., Andrade, M. F., Fattori, A. P.: Preliminary studies of the effect of aerosols on nitrogen dioxide photolysis rates in the city of Sao Paulo, Brazil. ATMOSPHERIC RESEARCH, 75, 135–148, 10.1016/j.atmosres.2004.12.004, 2005.

Daumont, D., Brion, J., Charbonnier, J., Malicet, J.: Ozone UV spectroscopy I: absorption cross-sections at room temperature. JOURNAL OF ATMOSPHERIC CHEMISTRY, 15, 145-155, 1992.

Davenport, J.E.: Determination of NO_2 photolysis parameters for stratospheric modelling, FAA Report No, FAA-EQ-7-14, 1978.

Dickerson, R. R., Kondragunta, S., Stenchikov, G., Civerolo, K. L., Doddridge, B. G., Holben, N.: The impact of aerosols on solar ultraviolet radiation and photochemical smog, SCIENCE, 278, 827–830, 10.1126/science.278.5339.827, 1997.

Ehhalt, D. H., Rohrer, F.: Dependence of the OH concentration on solar UV, JOURNAL OF GEOPHYSICAL RESEARCH-ATMOSPHERES, 105**,** 3565-3571, 10.1029/1999JD901070, 2000.

Eskes, H. J., Van Velthoven, P. F. J., Valks, P. J. M., Kelder, H. M.: Assimilation of GOME total ozone satellite observations in a three-dimensional tracer transport model, QUARTERLY JOURNAL OF THE ROYAL METEOROLOGICAL SOCIETY. 129, 1663-1681, doi:10.1256/qj.02.14, 2003.

743 Finlayson-Pitts, B. J., Pitts, J. N.: Chemistry of the Upper and Lower Atmosphere.
744 Academic Press, New York, 2000.
745 Flynn, J., Lefer, B., Rappenglück, B., Leuchner, M., Perna, R., Dibb, J., Ziemba, L.,
746 Anderson, C., Stutz, J., Brune, W., Ren, X. R.: Impact of clouds and aerosols on
747 ozone production in Southeast Texas. ATMOSPHERIC ENVIRONMENT, 44,
748 4126–4133, 10.1016/j.atmosenv.2009.09.005, 2010.
749 Fotiadi, A., Hatzianastassiou, N., Drakakis, E., Matsoukas, C., Pavlakis, K. G.,
750 Hatzidimitriou, D., Gerasopoulos, E., Mihalopoulos, N., Vardavas, I.: Aerosol
751 physical and optical properties in the eastern Mediterranean Basin, Crete, from
752 Aerosol Robotic Network data, ATMOSPHERIC CHEMISTRY AND PHYSICS,
753 6, 5399–5413, 10.5194/acp-6-5399-2006, 2006
754 Gao W, Tie X X, Xu J M, Huang R J, Mao X Q, Zhou G Q, Luyu Chang.: Long-term
755 trend of O3 in a mega City (Shanghai), China: Characteristics, causes, and
756 interactions with precursors. SCIENCE OF THE TOTAL ENVIRONMENT, 603,
757 425–433, 10.1016/j.scitotenv.2017.06.099, 2017.
758 Garland, R. M., Schmid, O., Nowak, A., Achtert, P., Wiedensohler, A., Gunthe, S. S.,
759 Takegawa, N., Kita, K., Kondo, Y., Hu, M.: Aerosol optical properties observed
760 during Campaign of Air Quality Research in Beijing 2006 (CAREBeijing-2006):
761 Characteristic differences between the inflow and outflow of Beijing city air,
762 JOURNAL OF GEOPHYSICAL RESEARCH-ATMOSPHERES, 114, D00G04,
763 10.1029/2008JD010780, 2009.
764 Gerasopoulos, E., Kazadzis, S., Vrekoussis, M., Kouvarakis, G., Liakakou, E.,
765 Kouremeti, N., Giannadaki, D., Kanakidou, M., Bohn, B., Mihalopoulos, N.:
766 Factors affecting O_3 and NO_2 photolysis frequencies measured in the eastern
767 Mediterranean during the five-year period 2002–2006, JOURNAL OF
768 GEOPHYSICAL RESEARCH-ATMOSPHERES, 117, D22305,
769 10.1029/2012JD017622, 2012.
770 Goliff, W. S., Stockwell, W. R., Lawson, C. V.: The regional atmospheric chemistry
771 mechanism, version 2, ATMOSPHERIC ENVIRONMENT, 68, 174–185,

772 10.1016/j.atmosenv.2012.11.038, 2013.
773 Guo, S., Hu M, Zamora, M. L., Peng, J. F., Shang, D. J., Zheng, J., Du, Z. F., Wu, Z.
774 J., Shao, M., Zeng, L. M., Molina, M. J., Zhang, R. Y.: Elucidating severe urban
775 haze formation in China, PROCEEDINGS OF THE NATIONAL ACADEMY
776 OF SCIENCES OF THE UNITED STATES OF AMERICA, 111, 17373–17378,
777 10.1073/pnas.1419604111, 2014.
778 Han, T. T., Liu, X. G., Zhang, Y. H., Qu, Y., Gu, J. W., Ma, Q., Lu, K. D., Tian, H. Z,,
779 Chen, J., Zeng, L. M.: Characteristics of aerosol optical properties and their
780 chemical apportionments during CAREBeijing 2006, AEROSOL AND AIR
781 QUALITY RESEARCH,14: 1431-1442, 10.4209/aaqr.2013.06.0203, 2014.
782 Han, T. T., Xu, W. Q., Chen, C., Liu, X. G., Wang, Q. Q., Li, J., Zhao, X. J., Du, W.,
783 Wang, Z. F., Sun, Y. L.: Chemical apportionment of aerosol optical properties
784 during the Asia-Pacific Economic Cooperation summit in Beijing, China,
785 JOURNAL OF GEOPHYSICAL RESEARCH-ATMOSPHERES, 120,
786 10.1002/2015JD023918, 2015b.
787 Han, T. T., Xu, W. Q., Li, J., Freedman, A., Zhao, J., Wang, Q. Q., Chen, C., Zhang, Y.
788 J., Wang, Z. F., Fu, P. Q.: Aerosol optical properties measurements by a CAPS
789 single scattering albedo monitor: Comparisons between summer and winter in
790 Beijing, China, JOURNAL OF GEOPHYSICAL RESEARCH-ATMOSPHERES,
791 122, 2513-2526, 10.1002/2016JD025762, 2017.
792 Han, T., Liu, X., Zhang, Y., Qu, Y., Zeng, L., Hu, M., Zhu, T.: Role of secondary
793 aerosols in haze formation in summer in the Megacity Beijing, JOURNAL OF
794 ENVIRONMENTAL SCIENCES, 31, 51-60, 10.1016/j.jes.2014.08.026, 2015a.
795 Harker, A. B., Ho, W., and Ratto, J. J.: Photodissociation quantum yields of NO_2 in
796 the region 375 to 420 nm, CHEMICAL PHYSICS LETTERS. 50, 394-397,
797 1977.
798 He, S., Carmichael, G. R.: Sensitivity of photolysis rates and ozone production in the
799 troposphere to aerosol properties, JOURNAL OF GEOPHYSICAL
800 RESEARCH-ATMOSPHERES, 104, 26307–26324, 10.1029/1999JD900789,

1999.

Hendrick, F; Muller, JF; Clemer, K; Wang, P; De Maziere, M; Fayt, C; Gielen, C; Hermans, C; Ma, JZ; Pinardi, G ; Stavrakou, T; Vlemmix, T; Van Roozendael, M., Four years of ground-based MAX-DOAS observations of HONO and NO_2 in the Beijing area. ATMOSPHERIC CHEMISTRY AND PHYSICS, 14(2), 765-781, 2014.Hodzic, A., Madronich, S., Bohn, B., Massie, S., Menut, L., and Wiedinmyer, C.: Wildfire particulate matter in Europe during summer 2003: meso-scale modeling of smoke emissions, transport and radiative effects, ATMOSPHERIC CHEMISTRY AND PHYSICS, 7, 4043–4064, 10.5194/acp-7-4043-2007, 2007.

Hofzumahaus, A., Kraus, A., Muller, M.: Solar actinic flux spectroradiometry: A technique for measuring photolysis frequencies in the atmosphere, APPLIED OPTICS, 38, 4443–4460, 10.1364/AO.38.004443, 1999.

Hofzumahaus, A., Lefer, B. L., Monks, P. S., Hall, S. R., Kylling, A., Mayer, B., Shetter, R. E., Junkermann, W., Bais, A., Calvert, J. G., Cantrell, C. A., Madronich, S., Edwards, G. D., Kraus, A.: Photolysis frequency of O_3 to $O(^1D)$: Measurements and modeling during the International Photolysis Frequency Measurement and Modeling Intercomparison (IPMMI), JOURNAL OF GEOPHYSICAL RESEARCH-ATMOSPHERES, 109 (D8), D08S90, 10.1029/2003JD004333, 2004.

Jacobson, M, Z.: Studying the effects of aerosols on vertical photolysis rate coefficient and temperature profiles over an urban airshed, JOURNAL OF GEOPHYSICAL RESEARCH-ATMOSPHERES, 103, 10593–10604, 10.1029/98JD00287, 1998.

Jones, I. T. N. and Bayes, K.D. Photolysis of nitrogen dioxide, J. Chem. Phys. 59, 4836-4844, 1973.

Kazadzis, S., Bais, A. F., Balis, D., Zerefos, C. S., and Blumthaler, M. Retrieval of down-welling UV actinic flux density spectra from spectral measurements of global and direct solar UV irradiance, J. Geophys. Res., 105, 4857-4864, 2000.

Kazadzis, S., Topaloglou, C., Bais, A. F., Blumthaler, M., Balis, D., Kazantzidis, A., Schallhart, B. Actinic flux and O^1D photolysis frequencies retrieved from spectral measurements of irradiance at Thessaloniki, Greece, ATMOSPHERIC CHEMISTRY AND PHYSICS, 4, 2215-2226, DOI: 10.5194/acp-4-2215-2004, 2004.

Kazadzis, S., Amiridis, V., and Kouremeti, N. The Effect of Aerosol Absorption in Solar UV Radiation, Advances in Meteorology, Climatology and Atmospheric Physics, 1041-1047, 2012.

Krotkov, N., Bhartia, P. K., Herman, J., Slusser, J., Scott, G., Labow, G., Vasilkov, A. P., Eck, T. F., Dubovik, O., Holben, B. N. Aerosol ultraviolet absorption experiment (2000 to 2004), part 2: Absorption optical thickness, refractive index, and single scattering albedo, OPTICAL ENGINEERING, 44, 4, 041005. DOI: 10.1117/1.1886819, 2005. Kylling, A., Webb, A. R., Bais, A. F., Blumthaler, M., Schmitt, R., Thiel, S., Kazantzidis, A., Kift, R., Misslebeck, M., Schallhart, B., Schreder, J., Topaloglou, C., Kazadzis, S., and Rimmer, J.: Actinic flux determination from measurements of irradiance, JOURNAL OF GEOPHYSICAL RESEARCH, 108 (D16), 4506-4515, 2005.

Lefer, B. L., Shetter, R. E., Hall, S. R.: Impact of clouds and aerosols on photolysis frequencies and photochemistry during TRACE-P: 1. Analysis using radiative transfer and photochemical box models, JOURNAL OF GEOPHYSICAL RESEARCH-ATMOSPHERES, 108, 8821-8835, 10.1029/2002JD003171, 2003.

Li C C, Mao J T, Liu Q H. Using MODIS to study the distribution and seasonal variation of aerosol optical thickness in eastern China. SCIENCE BULLETIN (China), 48: 2094-2100. 2003.

Li, J., Wang, Z. F., Wang, X., Yamaji, K., Takigawa, M., Kanaya, Y., Pochanart, P., Liu, Y., Irie, H., Hu, B., Tanimoto, H., Akimoto, H.: Impacts of aerosols on summertime tropospheric photolysis frequencies and photochemistry over Central Eastern China, ATMOSPHERIC ENVIRONMENT, 45: 1817-1829, 10.1016/j.atmosenv.2011.01.016, 2011.

Liao, H., Yung, Y. L., and Seinfeld, J. H.: Effects of aerosols on tropospheric photolysis rates in clear and cloudy atmospheres, JOURNAL OF GEOPHYSICAL RESEARCH, 104(D19), 23697–23707, 1999.

Liu, Q.Y., Ma, T. M., Olson, M. R., Liu, Y. J., Zhang, T. T., Wu, Y., Schauer, J. J.: Temporal variations of black carbon during haze and non-haze days in Beijing, SCIENTIFIC REPORTS, 6, 33331, 10.1038/srep33331, 2016.

Liu, X. G., Zhang, Y. H., Jung, J. S., Gu, J. W., Li, Y. P., Guo, S., Chang, S. Y., Yue, D. L., Lin, P., Kim, Y. J., Hu, M., Zeng, L. M., Zhu, T.: Research on the hygroscopic properties of aerosols by measurement and modeling during CAREBeijing-2006. JOURNAL OF GEOPHYSICAL RESEARCH-ATMOSPHERES, 114, D00G16, DOI: 10.1029/2008JD010805.

Lou, S. J., Liao, H., Zhu, B.: Impacts of aerosols on surface-layer ozone concentrations in China through heterogeneous reactions and changes in photolysis rates. ATMOSPHERIC ENVIRONMENT, 85:123-138, 0.1016/j.atmosenv.2013.12.004, 2014.

Lu, K. D., Rohrer, F., Holland, F., Fuchs, H., Bohn, B., Brauers, T., Chang, C. C., Häseler, R., Hu, M., Kita, K., Kondo, Y., Li, X., Lou, S. R., Nehr, S., Shao, M., Zeng, L. M., Wahner, A., Zhang, Y. H., Hofzumahaus, A.: Observation and modelling of OH and HO_2 concentrations in the Pearl River Delta 2006: a missing OH source in a VOC rich atmosphere, ATMOSPHERIC CHEMISTRY AND PHYSICS, 12: 1541-1569, 10.5194/acp-12-1541-2012, 2012

Ma, X. Y., Wang, J. Y., Yu, F. Q., Jia, H. L., Hu, Y. N.: Can MODIS AOD be employed to derive PM2.5 in Beijing-Tianjin-Hebei over China? ATMOSPHERIC RESEARCH, 181, 250-256, 10.1016/j.atmosres.2016.06.018, 2016.

Ma, Z. W., Hu, X. F., Huang, L., Bi, J., Liu, Y.: Estimating Ground-Level $PM_{2.5}$ in China Using Satellite Remote Sensing. Environ Sci Technol, 48: 7436−7444.

Madronich, S.: The Atmosphere and UV-B Radiation at Ground Level, Environmental UV Photobiology, doi: 0.1007/978-1-4899-2406-3_1. 1993.

888 Madronich, S., and S. Flocke.: The role of solar radiation in atmospheric chemistry, in
889 Environmental Photochemistry, edited by P. Boule, pp. 1-26, Springer-Verlag,
890 New York, 1999.
891 Mailler, S., Menut, L., di Sarra, A. G., Becagli, S., Di Iorio, T., Bessagnet, B., Briant,
892 R., Formenti, P., Doussin, J. F ., Gomez-Amo, J. L., Mallet, M., Rea, G., Siour, G.,
893 Sferlazzo, D. M., Traversi, R., Udisti, R., Turquety, S.: On the radiative impact of
894 aerosols on photolysis rates: comparison of simulations and observations in the
895 Lampedusa island during the ChArMEx/ADRIMED campaign, ATMOSPHERIC
896 CHEMISTRY AND PHYSICS, 16(3):1219-1244, 10.5194/acp-16-1219-2016,
897 10.5194/acp-16-1219-2016, 2016.
898 Matsumi, Y., Comes, F.J., Hancock, G., Hofzumahaus, A., Hynes, A.J., Kawasaki, M.,
899 Ravishankara, A.R.: Quantum yields for production of $O(^1D)$ in the ultraviolet
900 photolysis of ozone: recommendation based on evaluation of laboratory data.
901 JOURNAL OF GEOPHYSICAL RESEARCH, 107 (D3), 4024.
902 doi:10.1029/2001JD000510. 2002.
903 Malicet, J., Daumont, D., Charbonnier, J., Parisse, C., Chakir, A., Brion, J.: Ozone UV
904 spectroscopy. II. Absorption cross-sections and temperature dependence.
905 JOURNAL OF ATMOSPHERIC Chemistry, 21 (3), 263-273, 1995.
906 Peeters, J., Nguyen, T. L., Vereecken, L.: HO_X radical regeneration in the oxidation of
907 isoprene. PHYSICAL CHEMISTRY CHEMICAL PHYSICS, 11: 5935-5939,
908 10.1039/b908511d, 2009.
909 Pere, J. C., Bessagnet, B., Pont, V., Mallet, M., Minvielle, F.: Influence of the
910 aerosol solar extinction on photochemistry during the 2010 Russian wildfires
911 episode, ATMOSPHERIC CHEMISTRY AND PHYSICS, 15**,** 10983-10998,
912 10.5194/acp-15-10983-2015, 2015.
913 Raga, G. B., Castro, T., Baumgardner, D.: The impact of megacity pollution on local
914 climate and implications for the regional environment: Mexico City,
915 ATMOSPHERIC ENVIRONMENT, 35, 1805-1811,
916 10.1016/S1352-2310(00)00275-2, 2001.

Real, E. and Sartelet, K.: Modeling of photolysis rates over Europe: impact on chemical gaseous species and aerosols, ATMOSPHERIC CHEMISTRY AND PHYSICS, 11, 1711–1727, 10.5194/acp-11-1711-2011, 2011.

Rohrer, F., Lu, K. D., Hofzumahaus, A., Bohn, B., Brauers, T., Chang, C. C., Fuchs, H., Haseler, R., Holland, F., Hu, M.: Maximum efficiency in the hydroxyl-radical-based self-cleansing of the troposphere, NATURE GEOSCIENCE, 7, 559-563, 2014.

Shetter, R. E., Muller, M.: Photolysis frequency measurements using actinic flux spectroradiometry during PEM-Tropics Mission: Instrumentation description and some results, JOURNAL OF GEOPHYSICAL RESEARCH-ATMOSPHERES, 104, 5647-5661, 10.1029/98JD01381, 1999.

Shetter, R. E.: Photolysis frequency of NO_2: measurement and modeling during the International Photolysis Frequency Measurement and Modeling Intercomparison (IPMMI), JOURNAL OF GEOPHYSICAL RESEARCH-ATMOSPHERES, 108, 8544, 10.1029/2002JD002932, 2003.

Stone, D; Whalley, L. K; Heard, D. E.: Tropospheric OH and HO_2 radicals: field measurements and model comparisons, Chem. Soc. Rev,41(19): 6348-6404, 10.1039/c2cs35140d, 2012.

Tang, Y., Carmichael, G. R., Kurata, G., Uno, I., Weber, R. J., Song, C. H., Guttikunda, S. K., Woo, J. H., Streets, D. G., Wei, C., Clarke, A. D., Huebert, B., Anderson, T. L.: Impacts of dust on regional tropospheric chemistry during the ACE-Asia experiment: a model study with observations, JOURNAL OF GEOPHYSICAL RESEARCH-ATMOSPHERES, 109, D19S21, 10.1029/2003JD003806, 2004.

Tian, P., Wang, G. F., Zhang, R. J., Wu, Y. F., Yan, P.: Impacts of aerosol chemical compositions on optical properties in urban Beijing, China, PARTICUOLOGY, 18, 155-164, 10.1016/j.partic.2014.03.014, 2015.

Tie, X. X., Madronich, S., Walters, S., Edwards, D. P., Ginoux, P., Mahowald, N., Zhang, R. Y., Lou, C., Brasseur, G.: Assessment of the global impact of aerosols on tropospheric oxidants. JOURNAL OF GEOPHYSICAL

946 RESEARCH-ATMOSPHERES, 110, D03204, 10.1029/2004JD005359, 2005.
947 Topaloglou, C., Kazadzis, S., Bais, AF., Blumthaler, M., Schallhart, B., Balis, D.: NO_2
948 and HCHO photolysis frequencies from irradiance measurements in Thessaloniki,
949 Greece. ATMOSPHERIC CHEMISTRY AND PHYSICS, 5, 1645-1653, DOI:
950 10.5194/acp-5-1645-2005, 2005.
951 Trebs, I., Bohn, B., Ammann, C., Rummel, U., Blumthaler, M., Konigstedt, R.,
952 Meixner, F. X ., Fan, S., Andreae, M. O.: Relationship between the NO_2
953 photolysis frequency and the solar global irradiance, ATMOSPHERIC
954 MEASUREMENT TECHNIQUES, 2, 725-739, DOI: 10.5194/amt-2-725-2009,
955 2009.
956 van Donkelaar, A., Martin, R. V., Brauer, M., Kahn, R., Levy, R., Verduzco, C., and
957 Villeneuve, P. J.: Global Estimates of Ambient Fine Particulate Matter
958 Concentrations from Satellite-Based Aerosol Optical Depth: Development and
959 Application. Environmental Health Perspectives, 118, 847-855,
960 10.1289/ehp.0901623, 2010.
961 Verstraeten, W, W., Neu, J. L., Williams, J. E., Bowman, K. W., Worden, J. R.,
962 Boersma, K. F.: Rapid increases in tropospheric ozone production and export
963 from China. NATURE GEOSCIENCE, 8, 690-695, 10.1038/NGEO2493, 2015.
964 Volkamer R, Sheehy P, Molina L T, Molina M J.: Oxidative capacity of the Mexico
965 City atmosphere – Part 1: A radical source perspective, ATMOSPHERIC
966 CHEMISTRY AND PHYSICS, 10, 6969–6991, 10.5194/acp-10-6969-2010,
967 2010.
968 Wang, B.,Shao, M., Lu, S. H., Yuan, B., Zhao, Y., Wang, M., Zhang, S. Q., Wu, D.:
969 Variation of ambient non-methane hydrocarbons in Beijing city in summer 2008,
970 ATMOSPHERIC CHEMISTRY AND PHYSICS, 10, 5911–5923,
971 10.5194/acp-10-5911-2010, 2010.
972 Wang, Q., Sun, Y., Jiang, Q., Du, W., Sun, C., Fu, P., Wang, Z.: Chemical
973 composition of aerosol particles and light extinction apportionment before and
974 during the heating season in Beijing, China. JOURNAL OF GEOPHYSICAL

RESEARCH-ATMOSPHERES, 120: 12,708-12,722, 10.1002/2015JD023871, 2015.

Xin, J. Y., Gong, C. S., Liu, Z. R., Cong, Z. Y., Gao, W. K., Song, T., Pan, Y. P., Sun, Y., Ji, D. S., Wang, L. L., Tang, G. Q.: Wang, Y. S.: The observation-based relationships between $PM_{2.5}$ and AOD over China, JOURNAL OF GEOPHYSICAL RESEARCH-ATMOSPHERES, 121, 10701-10716, 10.1002/2015JD024655, 2016.

Xu, J., Ma, J. Z., Zhang, X. L., Xu, X. B., Xu, X. F., Lin, W. L., Wang, Y., Meng, W., and Ma, Z. Q.: Measurements of ozone and its precursors in Beijing during summertime: impact of urban plumes on ozone pollution in downwind rural areas, ATMOSPHERIC CHEMISTRY AND PHYSICS, 11, 12241–12252, 10.5194/acp-11-12241-2011, 2011.

Zhang, J. P., Zhu, T., Zhang, Q. H., Li, C. C., Shu, H. L., Ying, Y., Dai, Z. P., Wang, X., Liu, X. Y., Liang, A. M., Shen, H. X., and Yi, B. Q.: The impact of circulation patterns on regional transport pathways and air quality over Beijing and its surroundings, ATMOSPHERIC. CHEMISTRY AND PHYSICS, 12, 5031–5053, 10.5194/acp-12-5031-2012, 2012.

Zhang, L., Shao, J., Lu, X., Zhao, Y., Hu, Y., Henze, D. K., Liao, H., Gong, S., Zhang, Q.: Sources and Processes Affecting Fine Particulate Matter Pollution over North China: An Adjoint Analysis of the Beijing APEC Period. ENVIRONMENTAL SCIENCE & TECHNOLOGY, 50(16), 8731-8740, 10.1021/acs.est.6b03010, 2016.

Zhang, Q., Yuan, B., Shao, M., Wang, X., Lu, S., Lu, K., Wang, M., Chen, L., Chang, C. C., Liu, S. C.: Variations of ground-level O3 and its precursors in Beijing in summertime between 2005 and 2011, ATMOSPHERIC CHEMISTRY AND PHYSICS, 14, 6089-6101, 10.5194/acp-14-6089-2014, 2014.

Zhang, R., Jing, J., Tao, J., Hsu, S. C., Wang, G., Cao, J., Lee, C. S. L., Zhu, L., Chen, Z., Zhao, Y., Shen, Z.: Chemical characterization and source apportionment of $PM_{2.5}$ in Beijing: seasonal perspective, ATMOSPHERIC CHEMISTRY AND

PHYSICS, 13, 7053-7074, 10.5194/acp-13-7053-2013, 2013.

Zheng, C. W., Zhao, C. F., Zhu, Y. N., Wang, Y., Shi, X. Q., Wu, X. L., Chen, T. M., Wu, F., Qiu, Y. M.: Analysis of influential factors for the relationship between $PM_{2.5}$ and AOD in Beijing, ATMOSPHERIC CHEMISTRY AND PHYSICS, 17, 13473-13489, 10.5194/acp-17-13473-2017, 2017.

Table 1. O_3 column concentration, temperature, relative humidity, daytime clear-sky fraction and respective standard deviation for different seasons (spring: March, April and May; summer: June, July and August; autumn: September, October and November; winter: December, January and February).

Season	O_3 column (Du)	Temperature (℃)	Relative humidity (%)	Clear-sky fraction(%)
Spring	355±37	16±7.8	33±18	41
Summer	310±24	28±4.2	57±18	36
Autumn	304±23	16±7.4	46±21	42
Winter	347±28	0.53±4.2	30±18	41

Table 2. Instruments deployed in the field campaign undertaken in August 2012 and used for data analysis.

Parameters	Measurement technique	Time resolution	Detection limit	Accuracy
$j(O^1D)$ and $j(NO_2)$	Spectroradiometer	10 s	/	± 10%
O_3	UV photometry	60 s	0.5 ppbv	± 5%
NO	Chemiluminescence	60 s	60 pptv	± 20%
NO_2	Chemiluminescence	60 s	300 pptv	± 20%
CO	IR photometry	60 s	4 ppb	± 5%
SO_2	Pulsed UV fluorescence	60 s	0.1 ppbv	± 5%
HCHO	Hantzsch fluorimetry	60 s	25 pptv	± 5%
VOCs	GC-FID/MS	1 h	20-300 pptv	± 15~20%

Table 3. Slope, intercept and the square of correlation coefficient (r^2) of linear fits of correlation between $j(O^1D)$ and AOD for each ozone column class at AOD smaller than 0.7.

	SZA=30°			SZA=60°		
O_3 column (DU)	Slope ($10^{-6}s^{-1}$)	Intercept ($10^{-6}s^{-1}$)	r^2	Slope ($10^{-6}s^{-1}$)	Intercept ($10^{-6}s^{-1}$)	r^2
300-330	-6.2±1.5	26±1	0.34	-4.2±0.4	7.7±0.3	0.41
330-360	-6.5±1.4	23±1	0.40	-5.0±0.3	7.1±0.2	0.52
360-390	-9.5±1.6	21±1	0.52	-6.9±0.6	7.6±0.3	0.66

Table 4. Slope, intercept and the square of correlation coefficient (r^2) of linear fits of correlation between $j(NO_2)$ and AOD for each ozone column class at AOD smaller than 0.7.

cos(SZA)	Slope (10^{-3} s^{-1})	Intercept (10^{-3} s^{-1})	r^2
0-0.2	-1.3±0.1	1.5±0.0	0.52
0.2-0.4	-2.4±0.1	3.4±0.0	0.41
0.4-0.6	-3.2±0.1	5.5±0.0	0.49
0.6-0.8	-2.1±0.1	7.2±0.1	0.38
0.8-1.0	-1.8±0.1	8.1±0.1	0.26

Table 5. The fitting parameters a_1-a_6 and determination coefficients of E5 for $j(NO_2)$.

a_1	a_2	a_3	a_4	a_5	a_6	r^2
		$\times 10^{-3}$				
-0.46 ± 0.05	-2.0 ± 0.03	13± 0.2	0.22± 0.01	0.32± 0.05	-4.0± 0.1	0.96

Table 6. The fitting parameters a_1-a_6 and determination coefficients of E6 for $j(O^1D)$ at ozone column range = 300-330 DU.

a_1	a_2	a_3	a_4	a_5	a_6	r^2
		$\times 10^{-6}$				
1.1 ± 0.3	0.58 ± 0.17	-8.7± 0.9	0.63 ± 0.05	-7.5 ± 0.3	43 ± 1	0.96

Table 7. Mean and standard deviation of observed data during daytime (6:00–18:00) for A day and B day.

Observed data	A day: August 21, 2012	B day: August 26, 2012
AOD	0.21 ± 0.05	3.2 ± 0.4
$PM_{2.5}$ ($\mu g\ m^{-3}$)	22 ± 9	125 ± 16
O_3 column (Du)	302 ± 3	301± 3
Temperature(°C)	28 ± 3	28 ± 3
Relative humidity (%)	48 ± 10	55 ± 12
$j(O^1D)(s^{-1})$	$1.6\times 0^{-5} \pm 1.2\times10^{-5}$	$6.9\times10^{-6} \pm 5.2\times10^{-6}$
$j(NO_2)(s^{-1})$	$5.4\times10^{-3} \pm 2.9\times10^{-3}$	$2.9\times10^{-3}\pm 1.7\times10^{-3}$
O_3 (ppb)	40 ± 17	87 ± 53
NO_2 (ppb)	11 ± 5	25± 10
CO (ppm)	0.24 ± 0.05	0.85 ± 0.14
VOC reactivity (s^{-1})	3.0 ± 0.7	6.4 ± 1.7
HCHO (ppb)	2.7± 1.1	7.4± 1.9

Table 8. Monthly mean and standard deviation of observed data during daytime (6:00–18:00) under the condition of AOD less than 1 and larger than 1 in August 2012

Observed data	AOD<1	AOD>1
AOD	0.43 ± 0.24	2.0 ± 0.8
$PM_{2.5}$ ($\mu g\ m^{-3}$)	26 ± 12	77 ± 47
O_3 column (Du)	303 ± 4	302 ± 5
Temperature(°C)	30 ± 4	29 ± 4
Relative humidity (%)	42 ± 16	57± 13
$j(O^1D)(s^{-1})$	$1.6\times10^{-5} \pm 1.1\times10^{-5}$	$1.0\times10^{-5} \pm 0.7\times10^{-5}$
$j(NO_2)(s^{-1})$	$5.6\times10^{-3} \pm 2.4\times10^{-3}$	$3.8\times10^{-3} \pm 1.7\times10^{-3}$
O_3 (ppb)	52 ± 34	68 ± 46
NO_2 (ppb)	16 ± 7.8	24 ± 9
CO (ppm)	0.47 ± 0.20	0.95 ± 0.47
VOC reactivity (s^{-1})	4.3 ± 1.7	6.2 ± 2.2
HCHO (ppb)	4.0 ± 1.4	6.5± 1.9

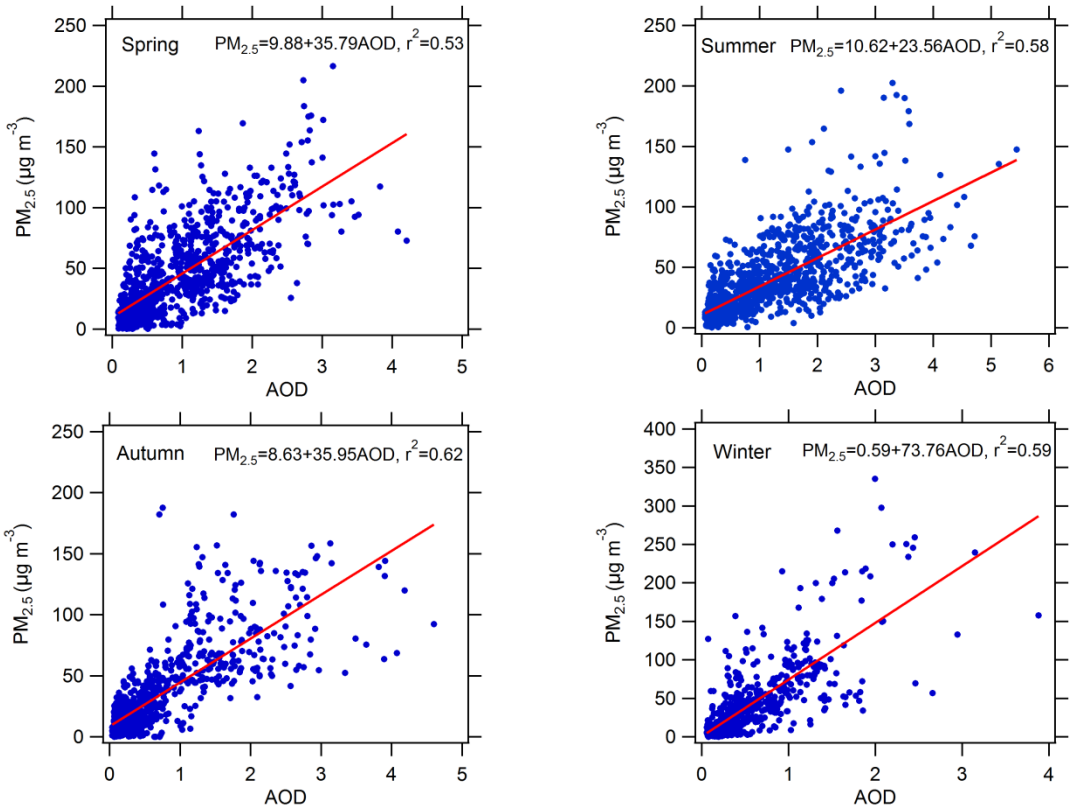

Figure 1. Scatter plots between AOD at 380nm and $PM_{2.5}$ in four different seasons. The slope, intercept and determination coefficient (r^2) were calculated.

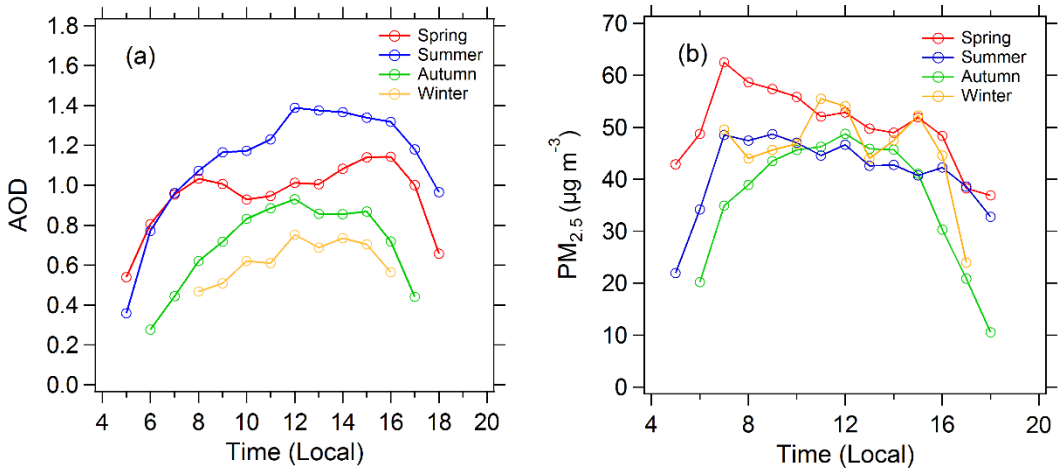

Figure 2. Diurnal cycles of (a) mean AOD and (b) mean $PM_{2.5}$ in the four seasons under cloudless conditions.

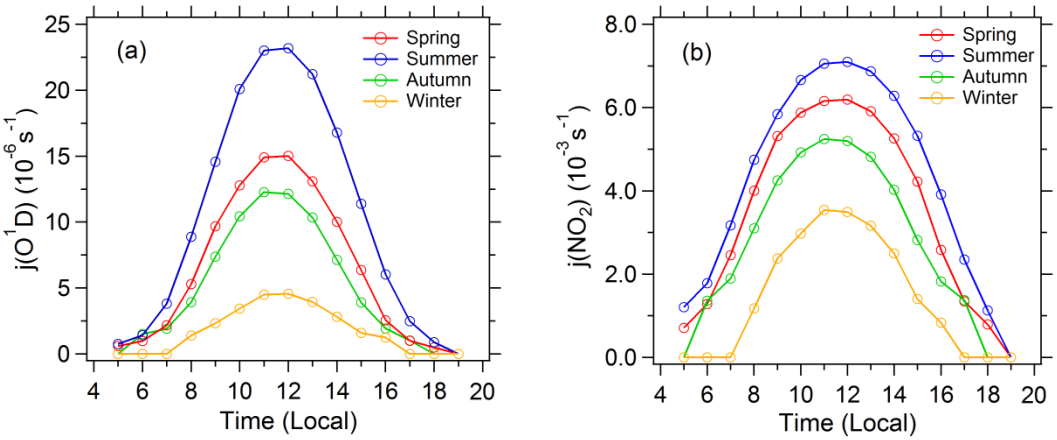

Figure 3. Diurnal cycles of (a) mean $j(O^1D)$ and (b) mean $j(NO_2)$ in the four seasons under cloudless conditions.

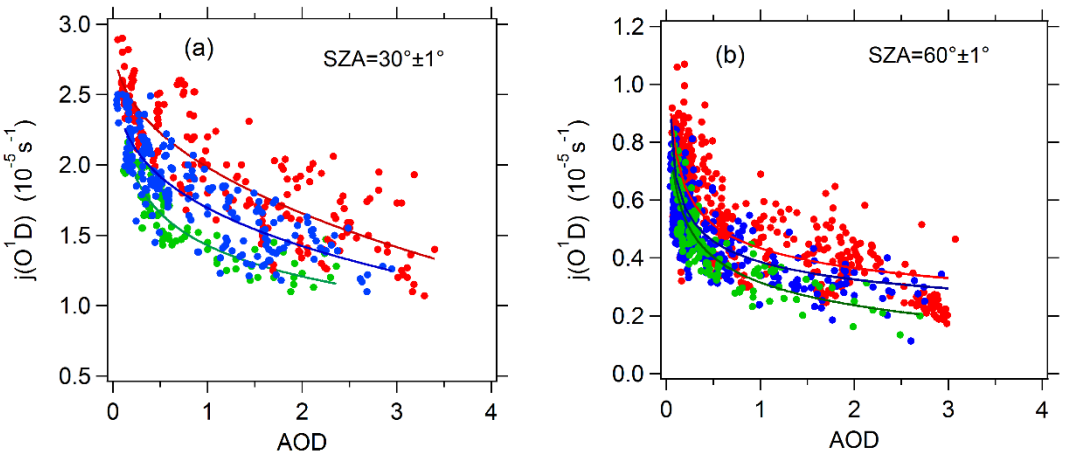

Figure 4. Dependence of $j(O^1D)$ on AOD (380nm) at SZA of (a) 30° and (b) 60° and at different classes of ozone column concentration: 300-330 DU (red), 330-360 DU (blue), and 360-390 DU (green). The full lines are fitted by exponential function.

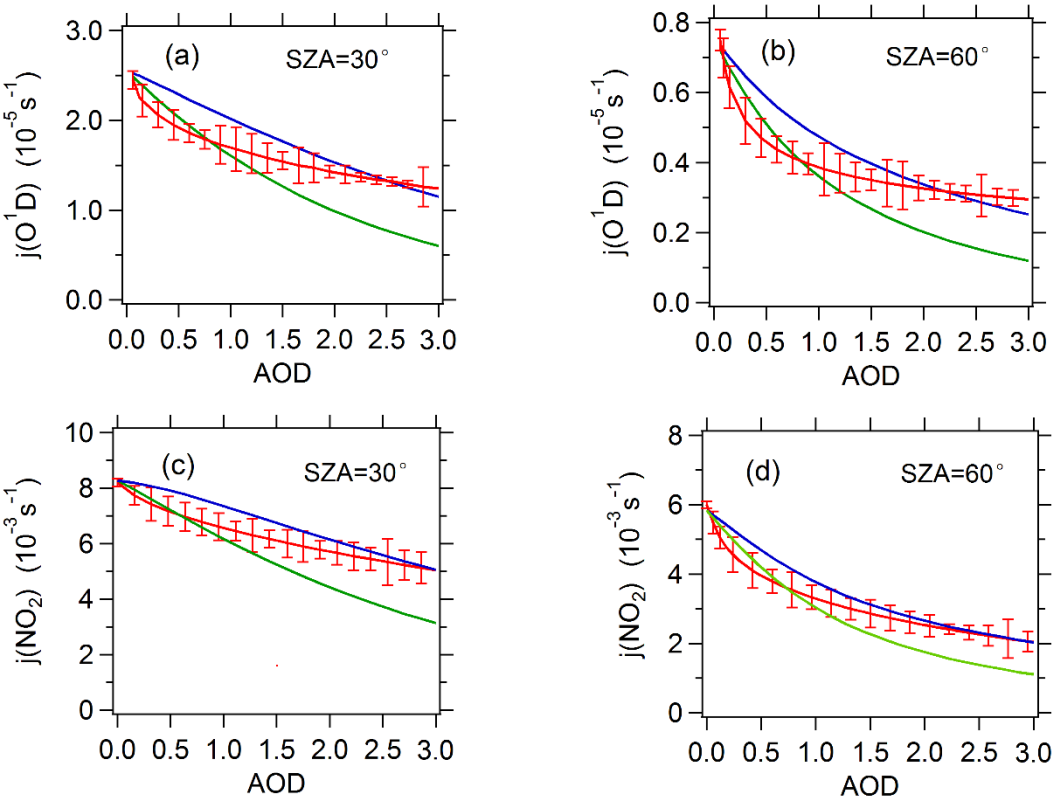

Figure 5. The relationship between observed or TUV-simulated photolysis frequencies and AOD (380nm) at SZA of 30° and 60°. For $j(O^1D)$, total ozone column classification of 330-360 DU is chosen. The red line represents observed average photolysis frequencies; the blue line and green line represents TUV-simulated average photolysis frequencies at SSA of 0.95 and 0.85 respectively.

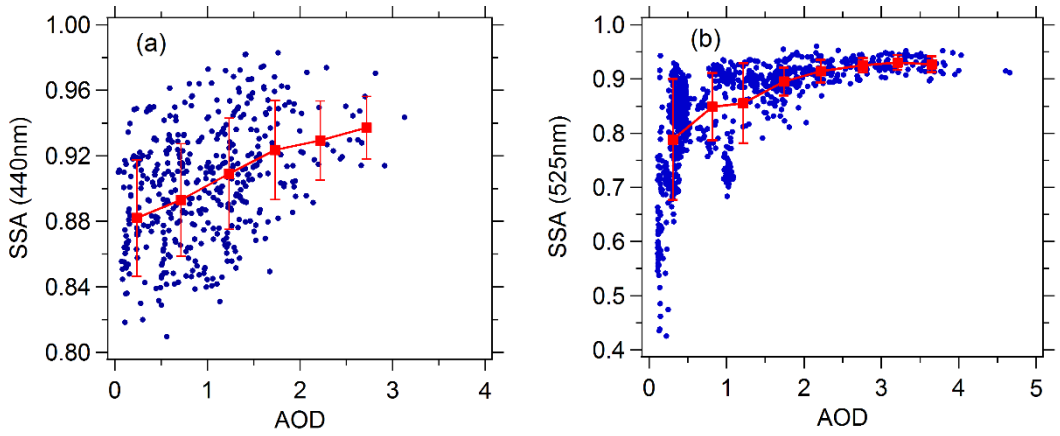

Figure 6. Correlation between SSA and AOD (380nm). (a) SSA (440nm) is acquired from AERONET during 2012-2015. (b) SSA (525nm) is acquired from near-ground measurement campaign in August 2012.

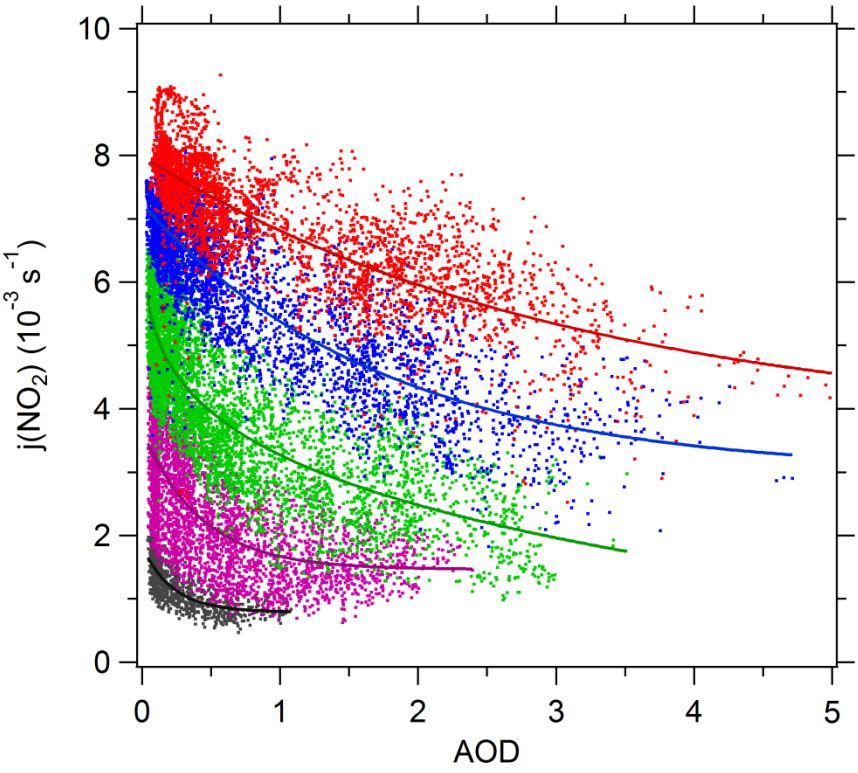

Figure 7. Dependence of $j(NO_2)$ on AOD (380nm) at different SZA classes. The classes of cos(SZA) are 0–0.2 (black), 0.2–0.4 (purple), 0.4–0.6 (green), 0.6–0.8 (blue), and 0.8–1 (red). The full lines are fitted by exponential function.

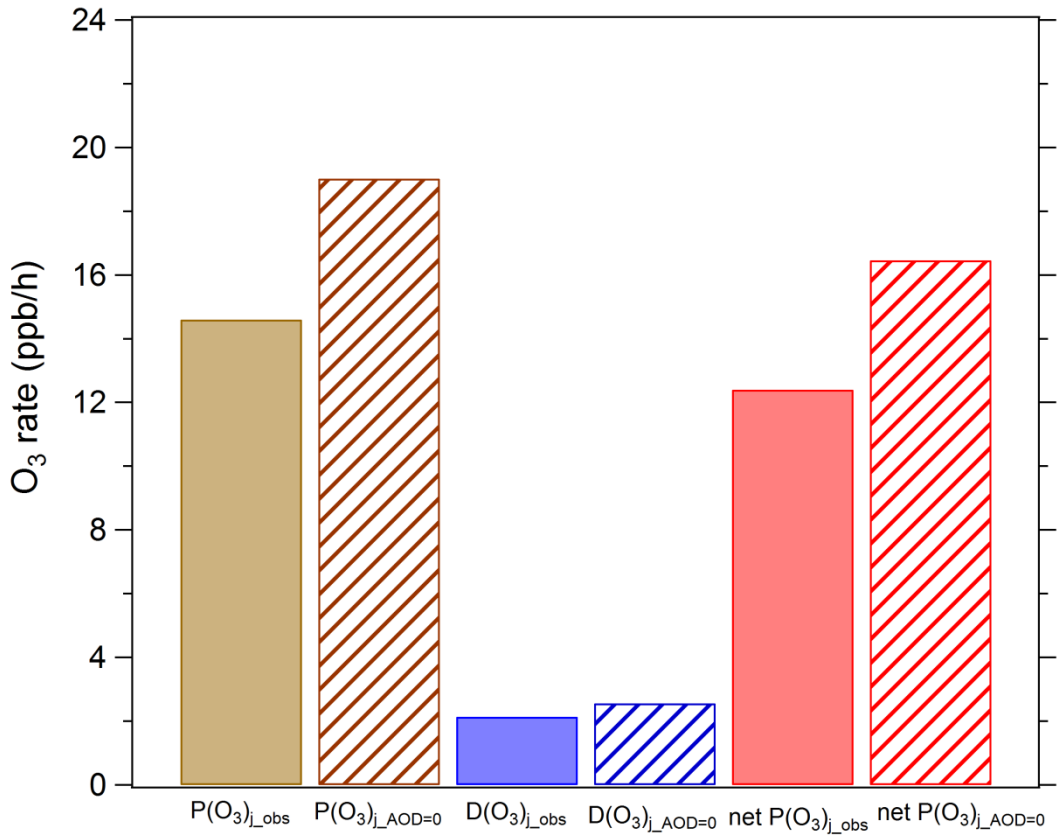

Figure 8. Mean daytime ozone production and loss terms in August 2012. $P(O_3)_{j\_obs}$, $D(O_3)_{j\_obs}$ and net $P(O_3)_{j\_obs}$ represents ozone production rate, ozone loss rate, and net ozone production rate under observed photolysis frequencies; $P(O_3)_{j\_AOD=0}$, $D(O_3)_{j\_AOD=0}$ and net $P(O_3)_{j\_AOD=0}$ represents ozone production rate, ozone loss rate, and net ozone production rate under calculated photolysis frequencies when AOD is equal to 0.

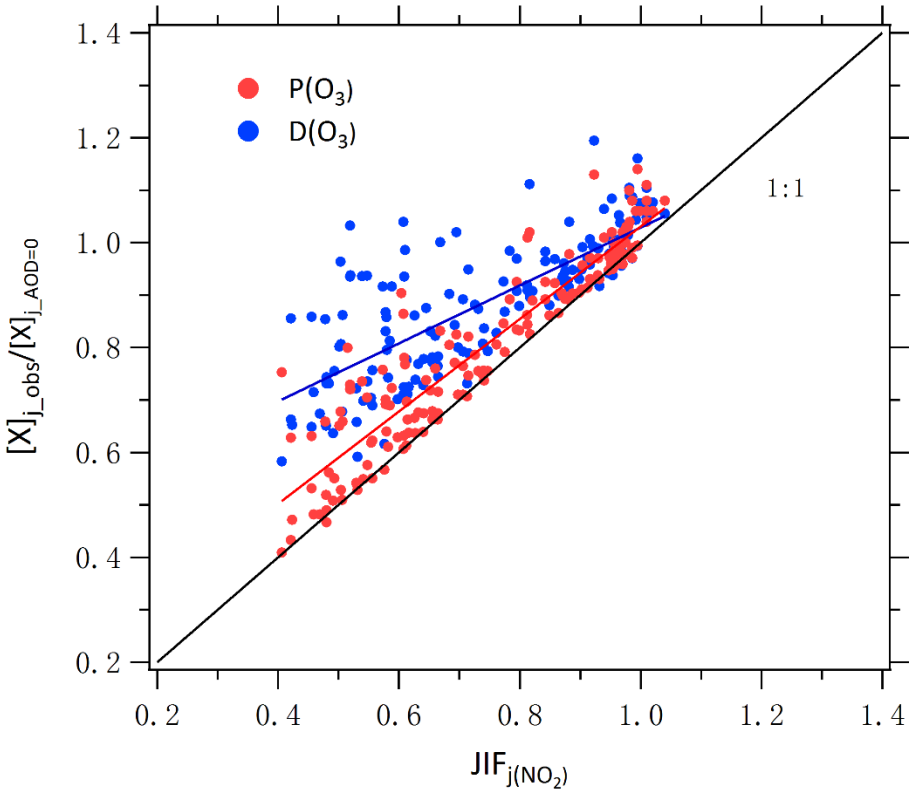

Figure 9. Correlation between $P(O_3)_{j\_obs}/P(O_3)_{j\_AOD=0}$ (or $D(O_3)_{j\_obs}/D(O_3)_{j\_AOD=0}$) and JIF of $j(NO_2)$. Single data point represent daytime hourly mean value.

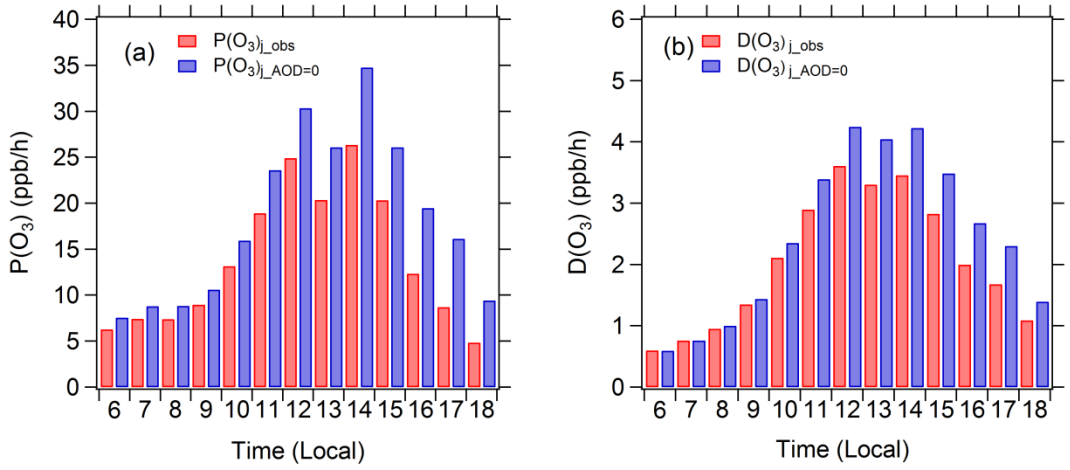

Figure 10. Diurnal profiles of mean $P(O_3)_{j\_obs}$, $P(O_3)_{j\_AOD=0}$, $D(O_3)_{j\_obs}$, and $D(O_3)_{j\_AOD=0}$ in August 2012 under clear-sky conditions.

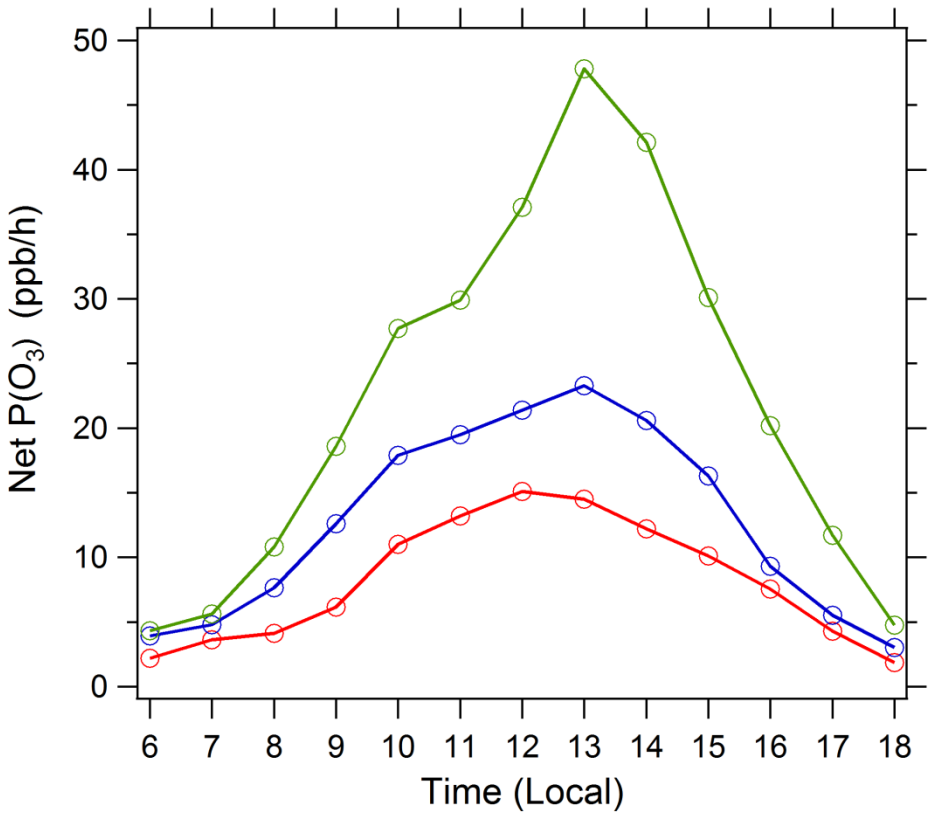

Figure 11. Diurnal profile of net $P(O_3)$ simulated by the box model. Three cases are displayed: (1) A day (red circles): August 21, 2012 with low AOD level and high photolysis frequencies; (2) B day (blue circles): August 26, 2012 with high AOD level and low photolysis frequencies; and (3) the photolysis frequencies of B day adjusted to the level of A day with other conditions unchanged (green circles). The specific conditions of A day and B day are listed in Table 7.

Supporting information

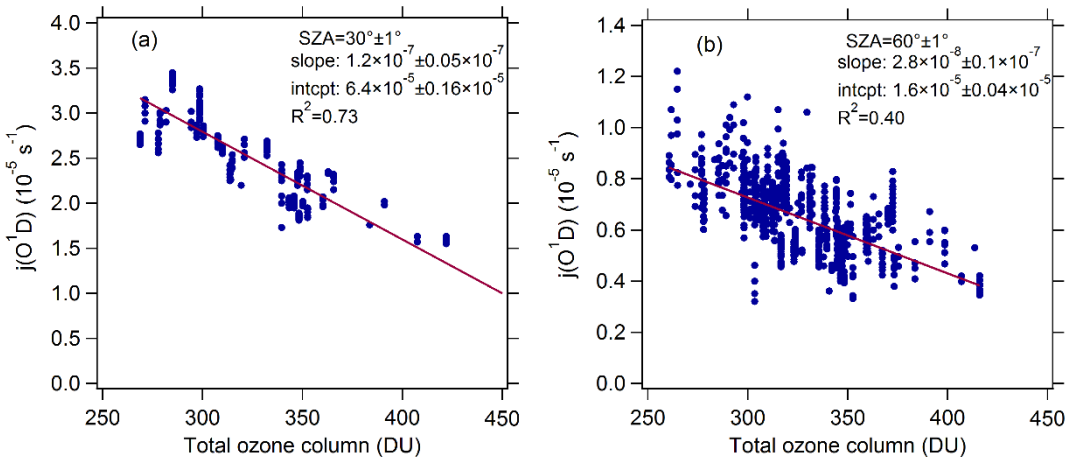

Figure S1. Dependence of $j(O^1D)$ on AOD (380nm) at low AOD level (AOD<0.3) and SZA of (a) 30°±1° and (b) 60°±1°, respectively.

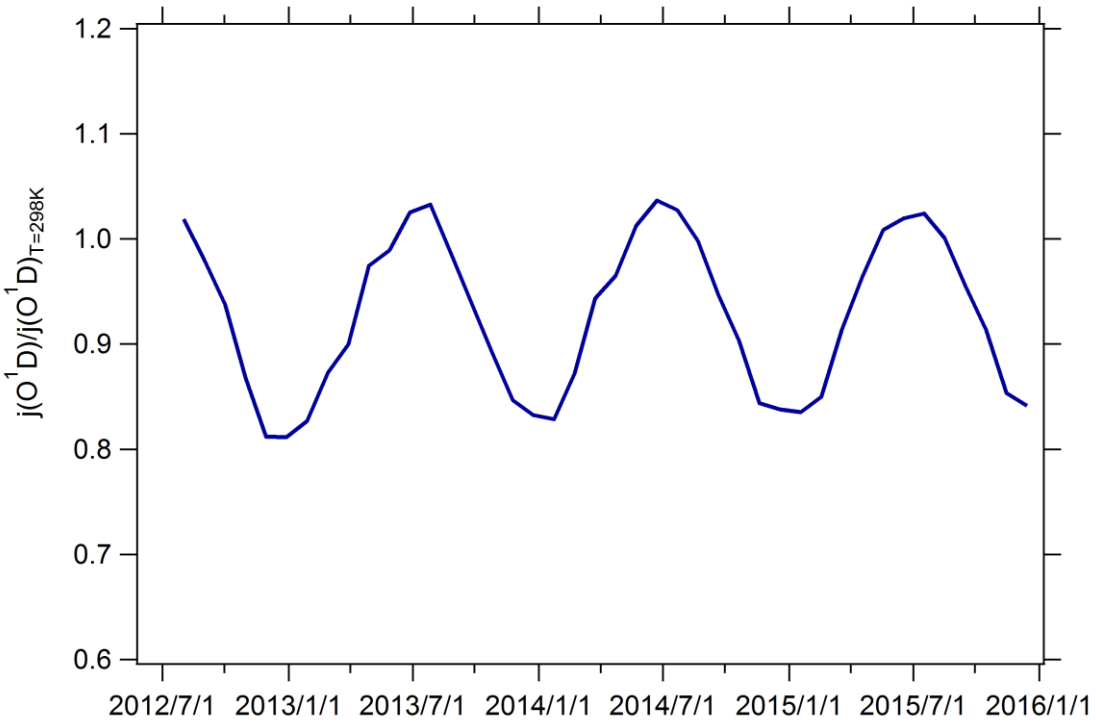

Figure S2. The time series of the monthly mean ratio of $j(O^1D)$ to $j(O^1D)_{T=298K}$ ($j(O^1D)/ j(O^1D)_{T=298K}$) from August 2012 to December 2015.

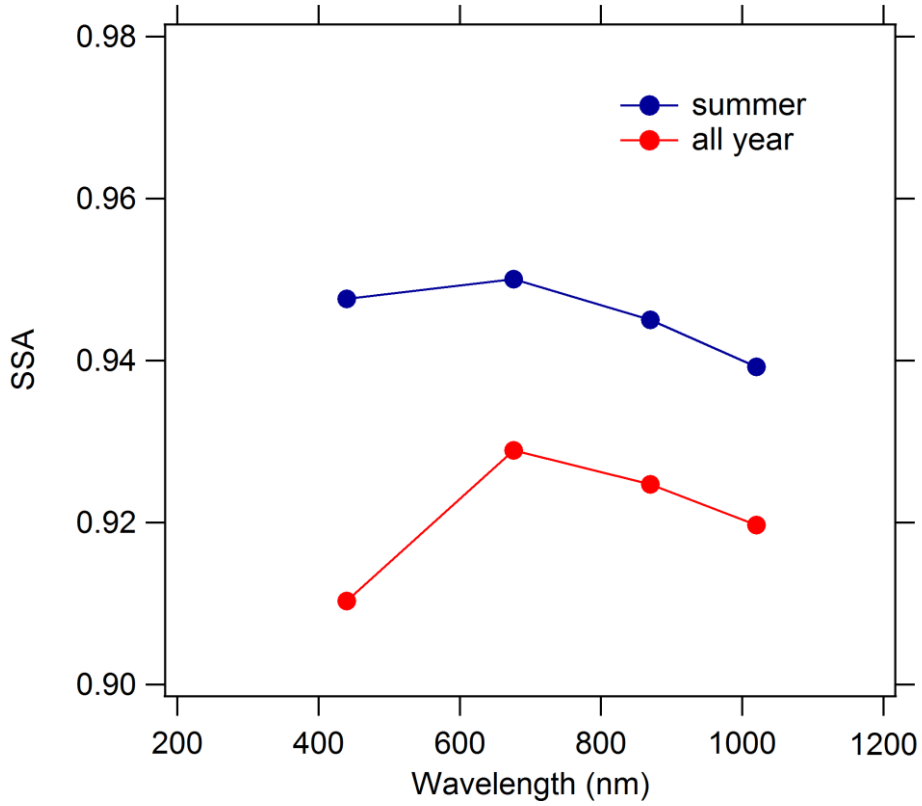

Figure S3. The dependence of AERONET based SSA on wavelength.

Table S1. The seasonal mean AOD and SSA of AERONET.

Seasons	Spring	Summer	Autumn	Winter
AOD	0.83±0.72	0.99±0.90	0.59±0.70	0.47±0.47
SSA	0.91±0.03	0.94±0.02	0.91±0.03	0.88±0.03